INTRODUCCION: PLANETAS EXTRASOLARES Y FORMACION PLANETARIA

Curso Planetología 2015

Tabaré Gallardo

www.astronomia.edu.uy/depto/planetologia/planet.html

exoplanets.org

Exoplanets Data Explorer | Methodology and FAQ | Exoplanets Links | California Planet Survey

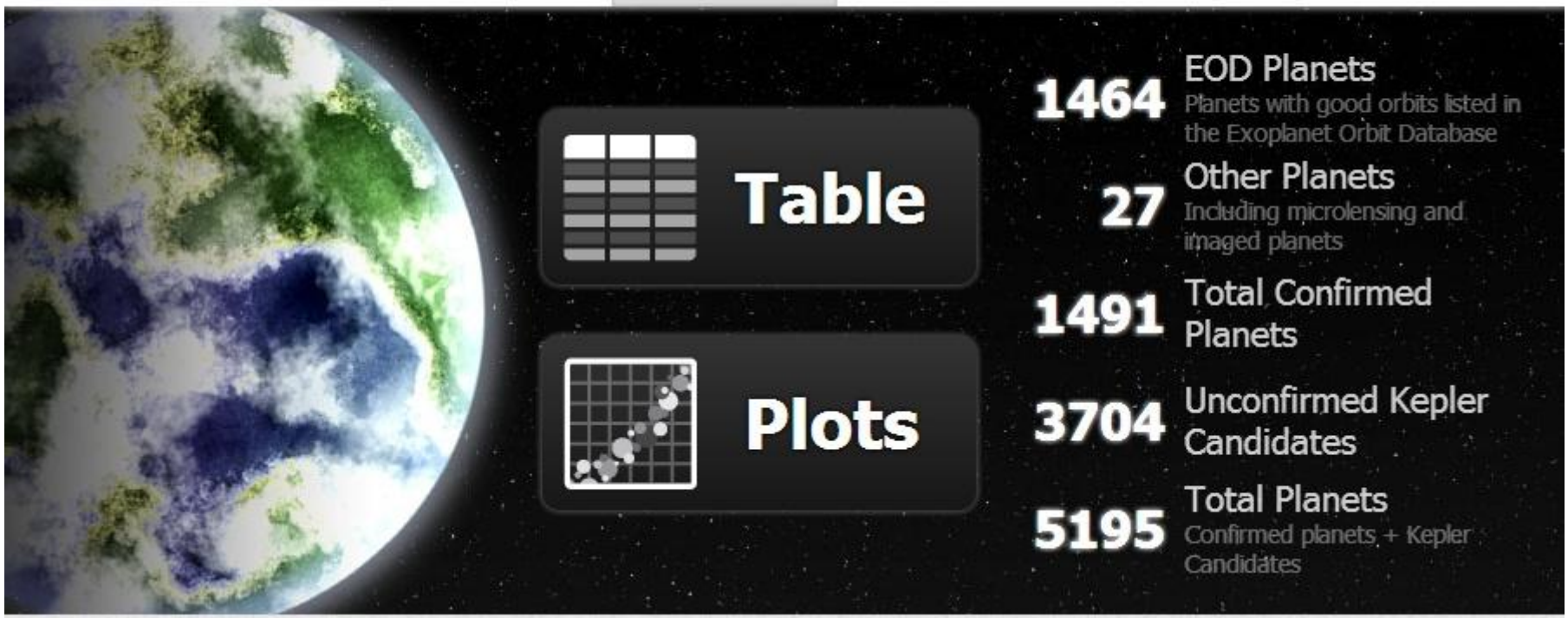

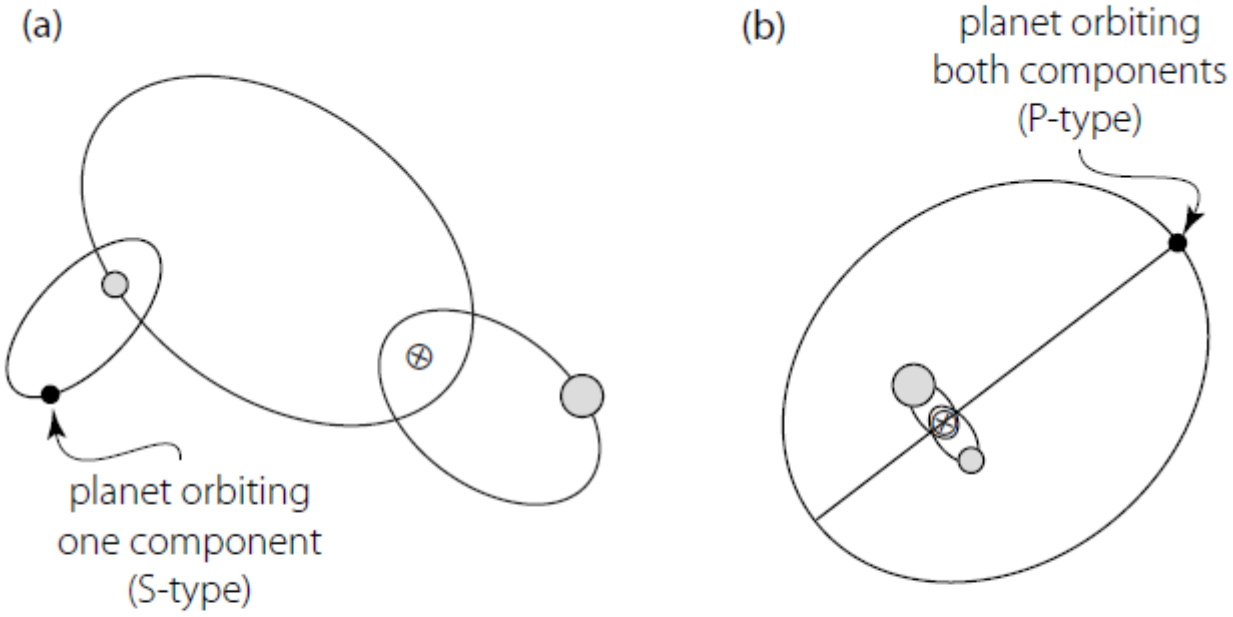

Figure 2.44: Schematic of a planet in a binary star system (⊗ indicates the stellar centre of mass): (a) the planet orbits one component of the stellar binary; (b) the planet is in a circumbinary orbit about both stellar components.

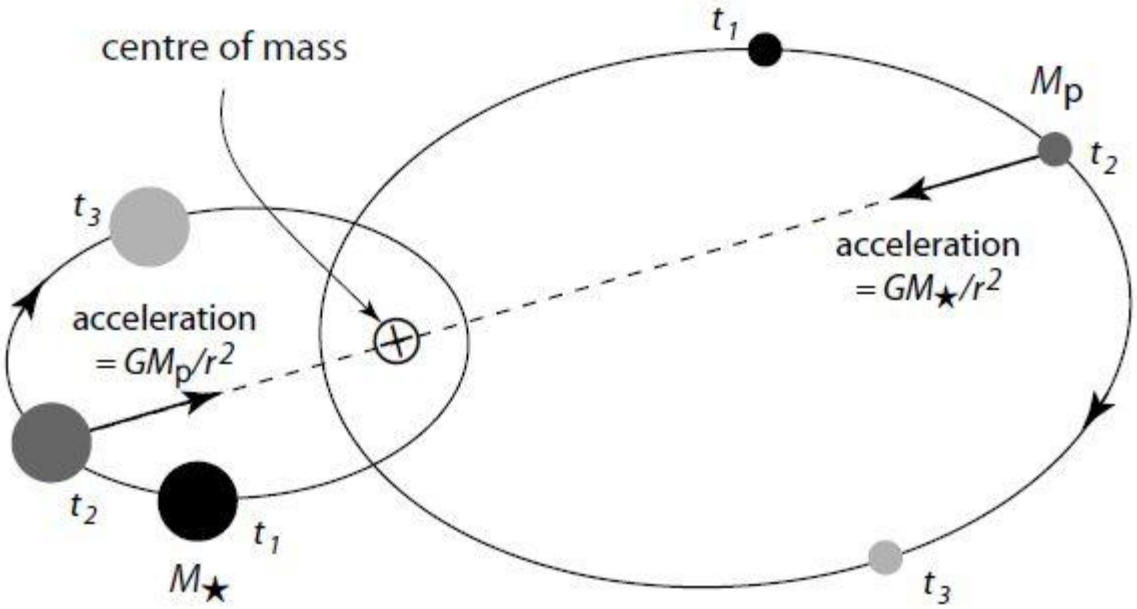

Figure 2.3: Two orbiting bodies, shown at times t_1, t_2, t_3, move about their common barycentre. Both bodies follow orbits having the same shape and period, but of different sizes and with ω differing by $180°$.

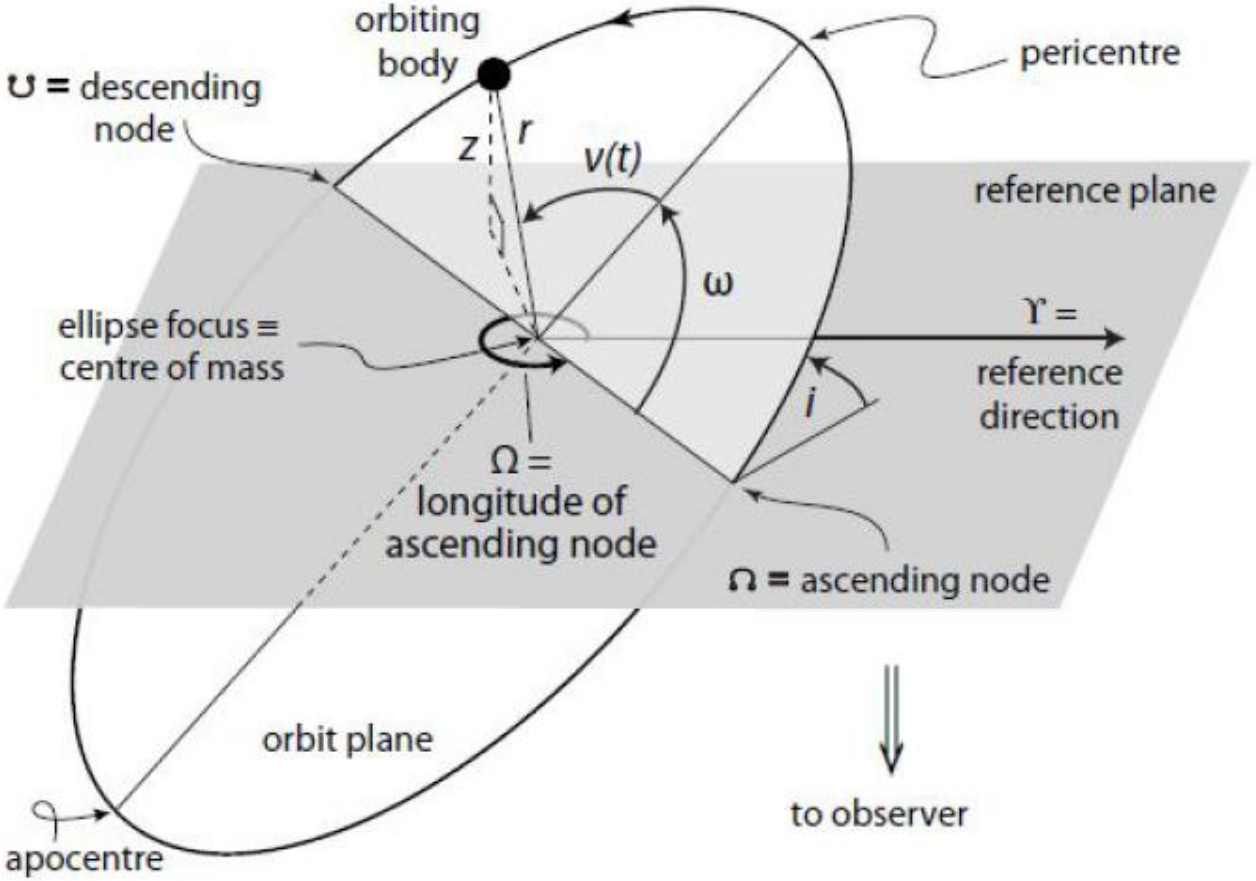

Figure 2.2: An elliptical orbit in three dimensions. The reference plane is tangent to the celestial sphere. i is the inclination of the orbit plane. The nodes are the points where the orbit and reference planes intersect. Ω defines the longitude of the ascending node, measured in the reference plane. ω is the fixed angle defining the object's argument of pericentre relative to the ascending node. The true anomaly, $\nu(t)$, is the time-dependent angle characterising the object's position along the orbit.

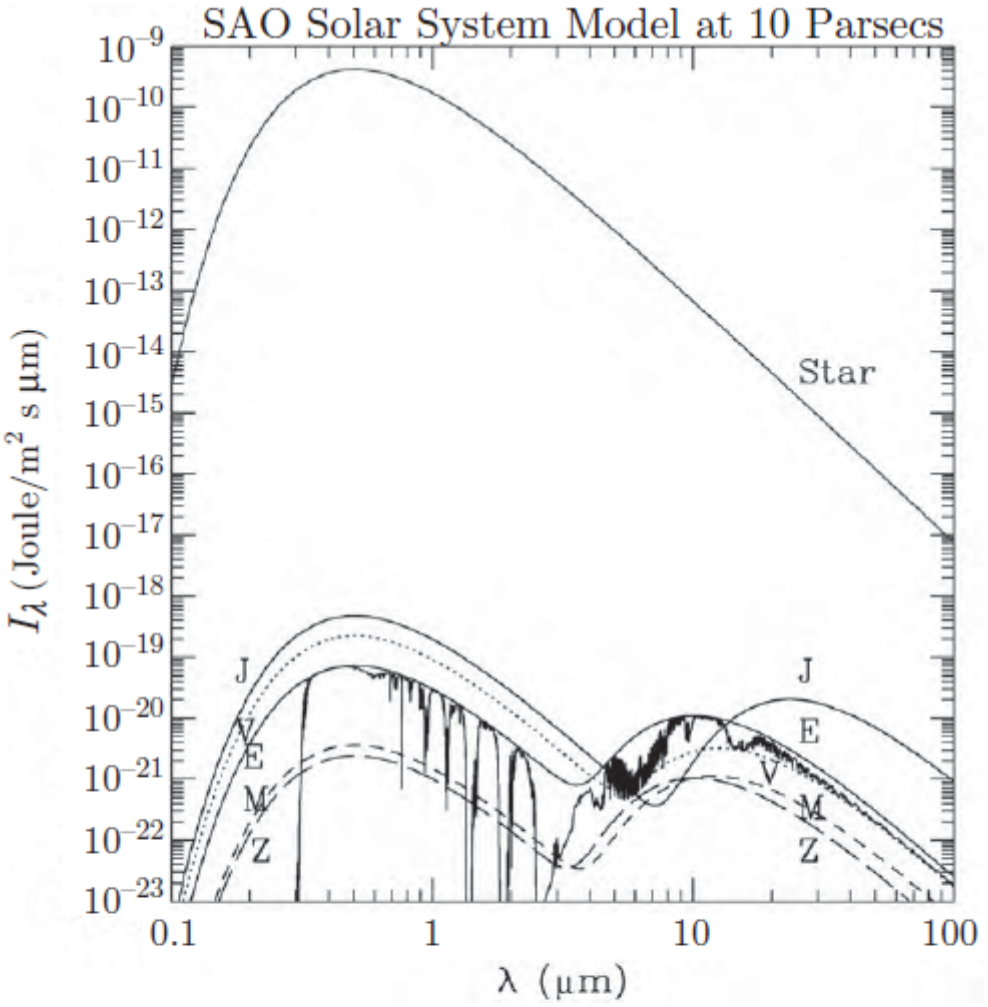

Figure 14.5 Spectral energy distribution of the Sun, Jupiter, Venus, Earth, Mars and the zodiacal cloud. The bodies are approximated by blackbodies of uniform albedo, with an additional curve showing Earth's atmospheric absorption features. (Adapted from Des Marais et al. 2002)

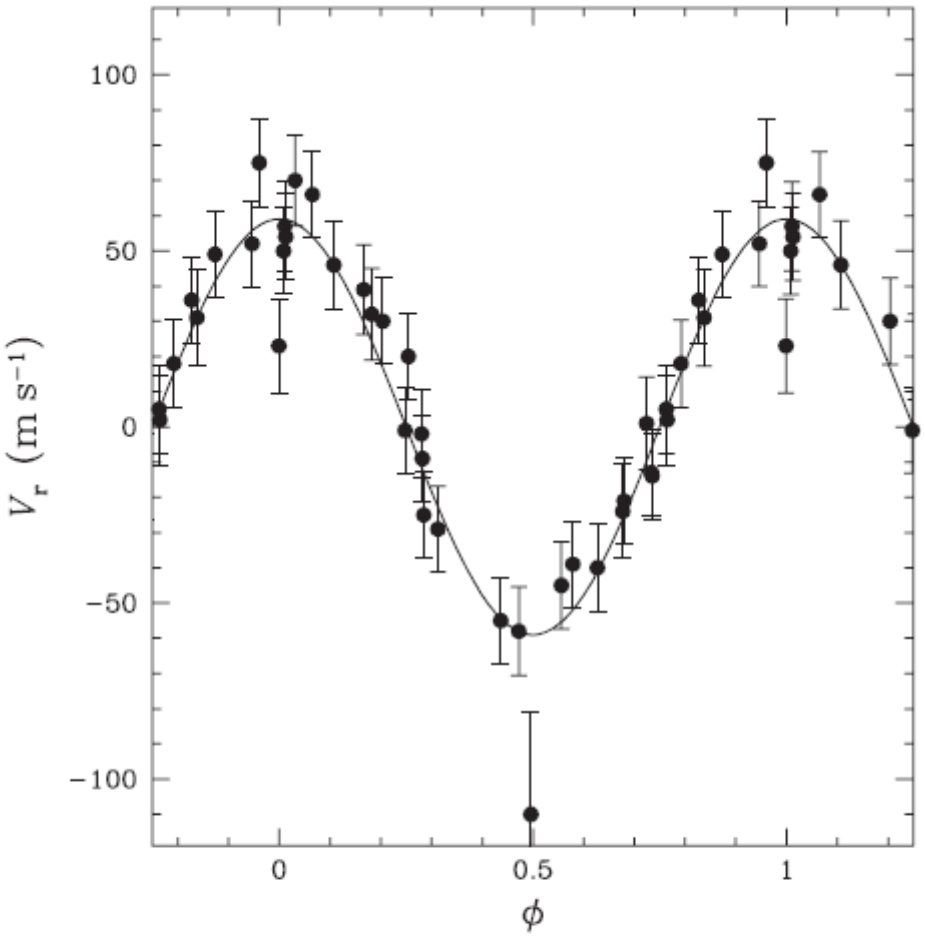

Figure 14.9 Radial velocity measurements of the star 51 Pegasi (*points with error bars*) as a function of phase of the orbital fit (*solid line*). These data were used to discover the first planet found around a main sequence star other than the Sun. One and a half cycles are shown for clarity. (Adapted from Mayor and Queloz 1995; courtesy Didier Queloz)

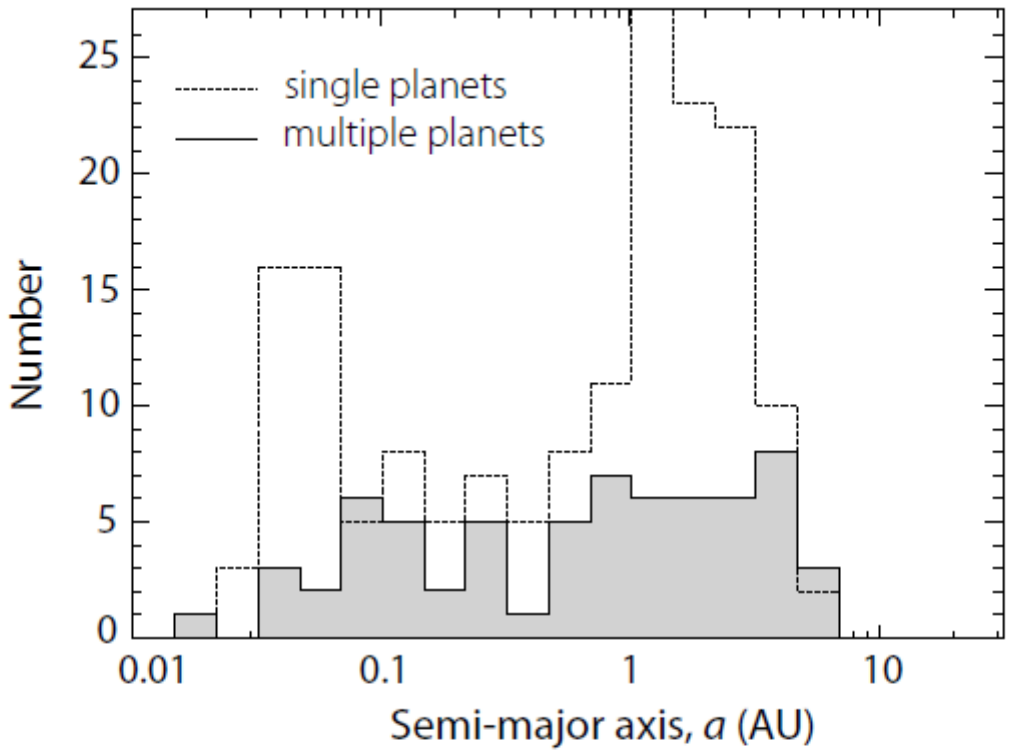

Figure 2.30: Distribution of semi-major axes for multiple planet systems (solid) and apparently single systems (dashed). The pile-up of hot Jupiters, and the jump in abundance beyond 1 AU seen in the single planet systems are not evident in the multiple planet systems. From Wright et al. (2009b, Figure 9), reproduced by permission of the AAS.

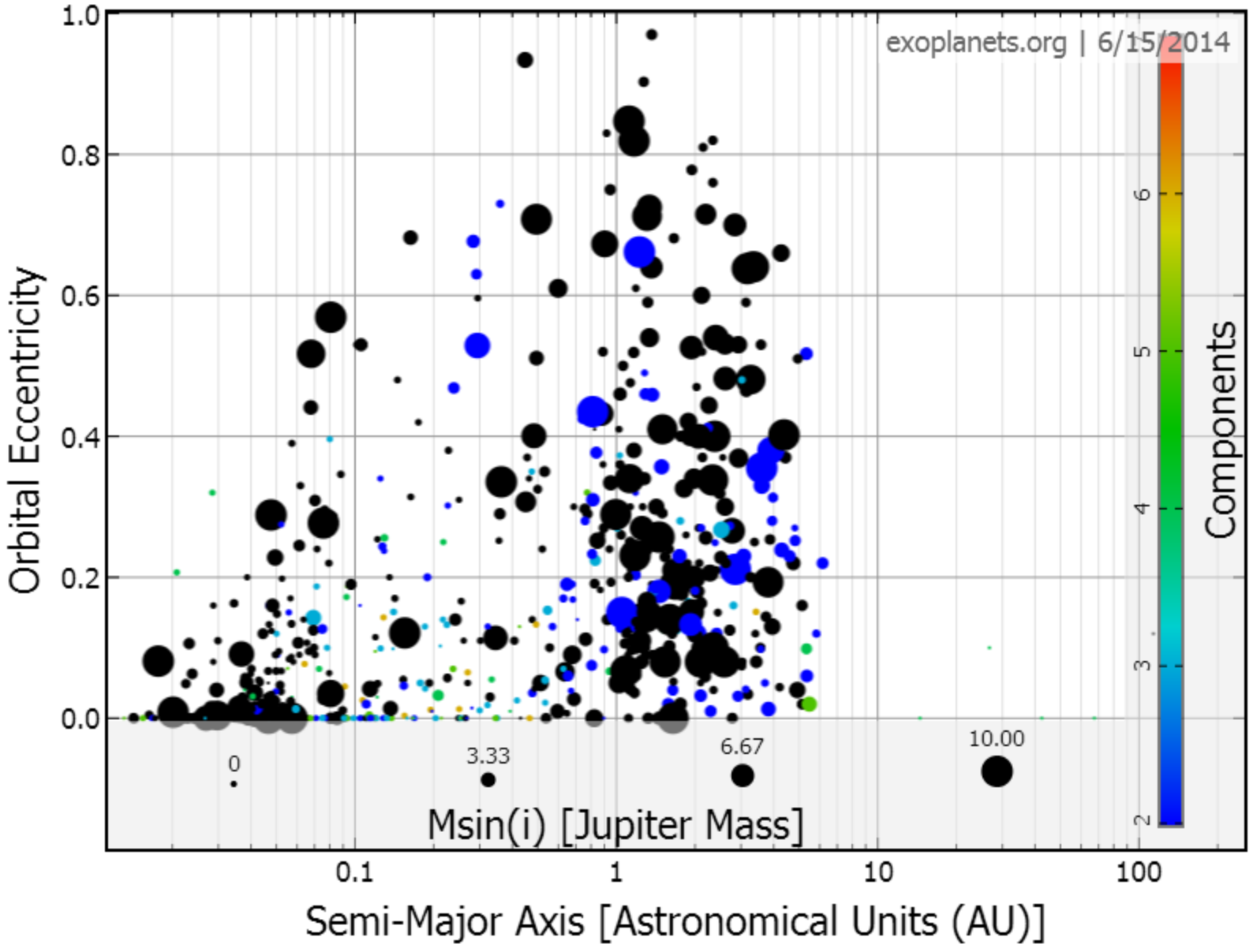
exoplanets.org | 6/15/2014
Orbital Eccentricity
1.0
0.8
0.6
0.4
0.2
0.0
Components
2
3
4
5
6
0
3.33
6.67
10.00
Msin(i) [Jupiter Mass]
0.1
1
10
100
Semi-Major Axis [Astronomical Units (AU)]

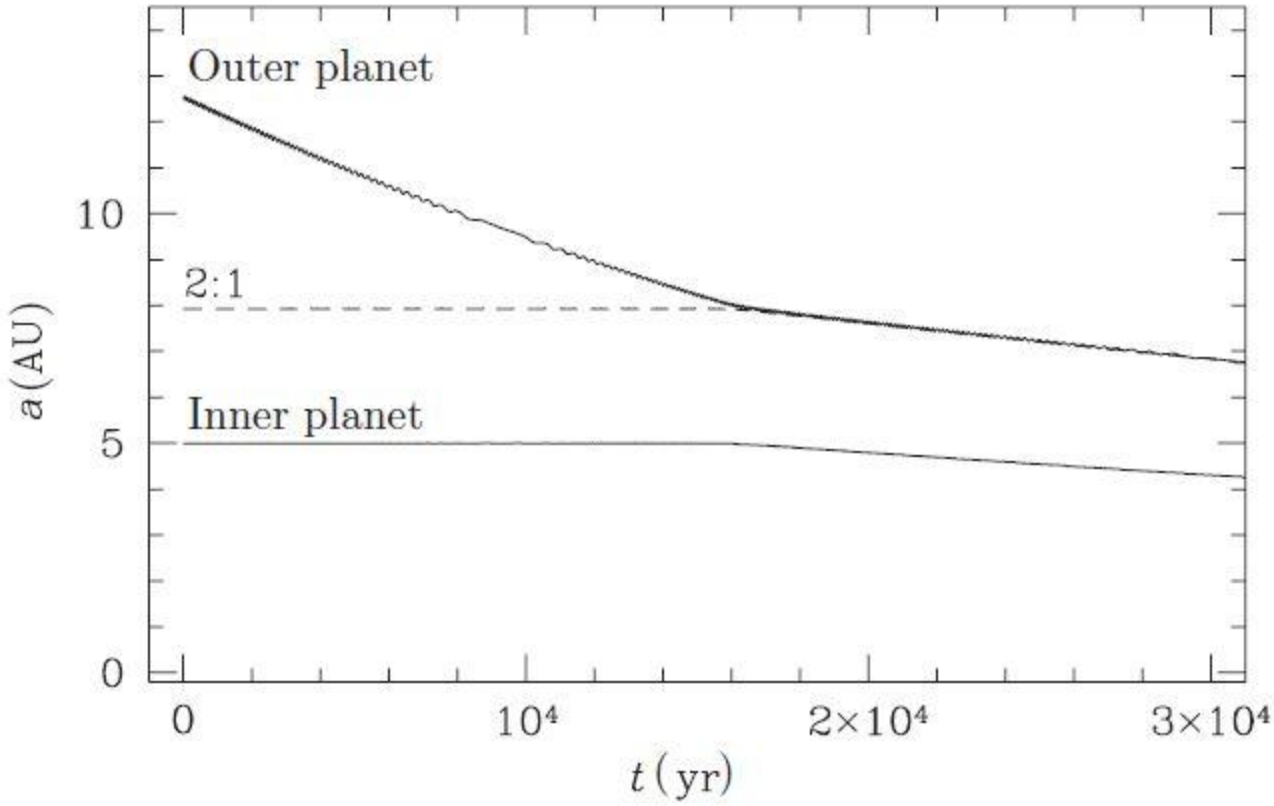

Fig. 7.5. Numerical example of resonant capture in a coplanar system of two initially well-separated Jupiter mass planets. For illustrative purposes the outer planet is subjected to a fictitious drag force which results in steady decay of its semi-major axis. The inner planet is almost unperturbed until the planets encounter their mutual 2:1 mean-motion resonance, at which point capture occurs and the two planets move inward in lockstep.

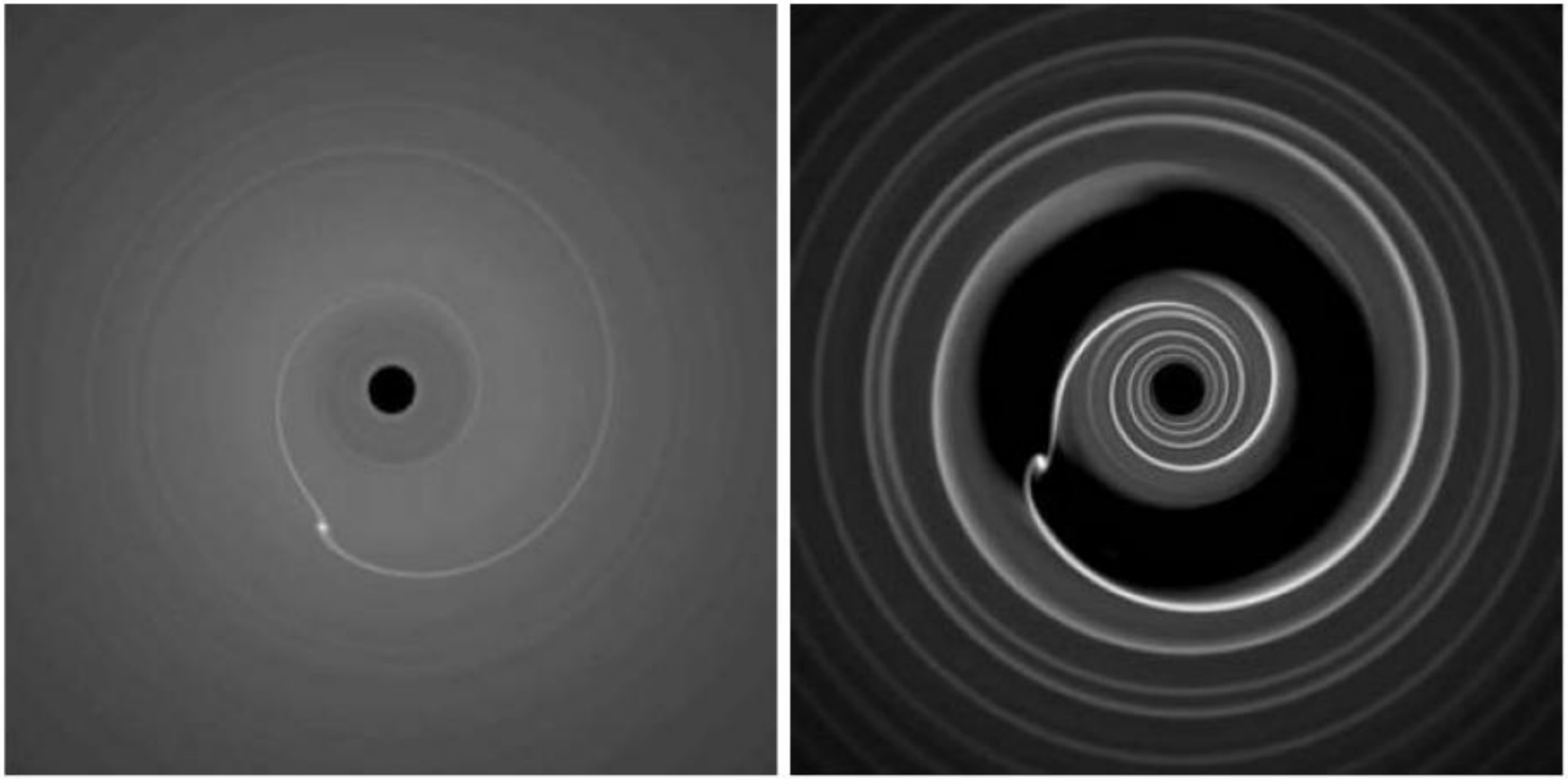

Fig. 7.1. Two-dimensional hydrodynamic simulations depicting the interaction between a planet and a viscous protoplanetary disk in (left panel) the Type 1 regime appropriate to low-mass planets and (right panel) the Type 2 regime relevant to giant planets. In both cases angular momentum exchange is the result of gravitational interaction with spiral waves set up within the disk as a consequence of the planetary perturbation. In the Type 1 regime the interaction is weak enough that the local surface density is approximately unperturbed, while in the Type 2 regime a strong interaction repels gas from the vicinity of the planet producing an annular gap.

SUPER-EARTHS RISING

Ground-based telescopes have detected around 650 planets from the wobble of their parent star. A new class of planet — between the size of Earth and Neptune — has emerged precisely where modellers have said planets shouldn't exist.

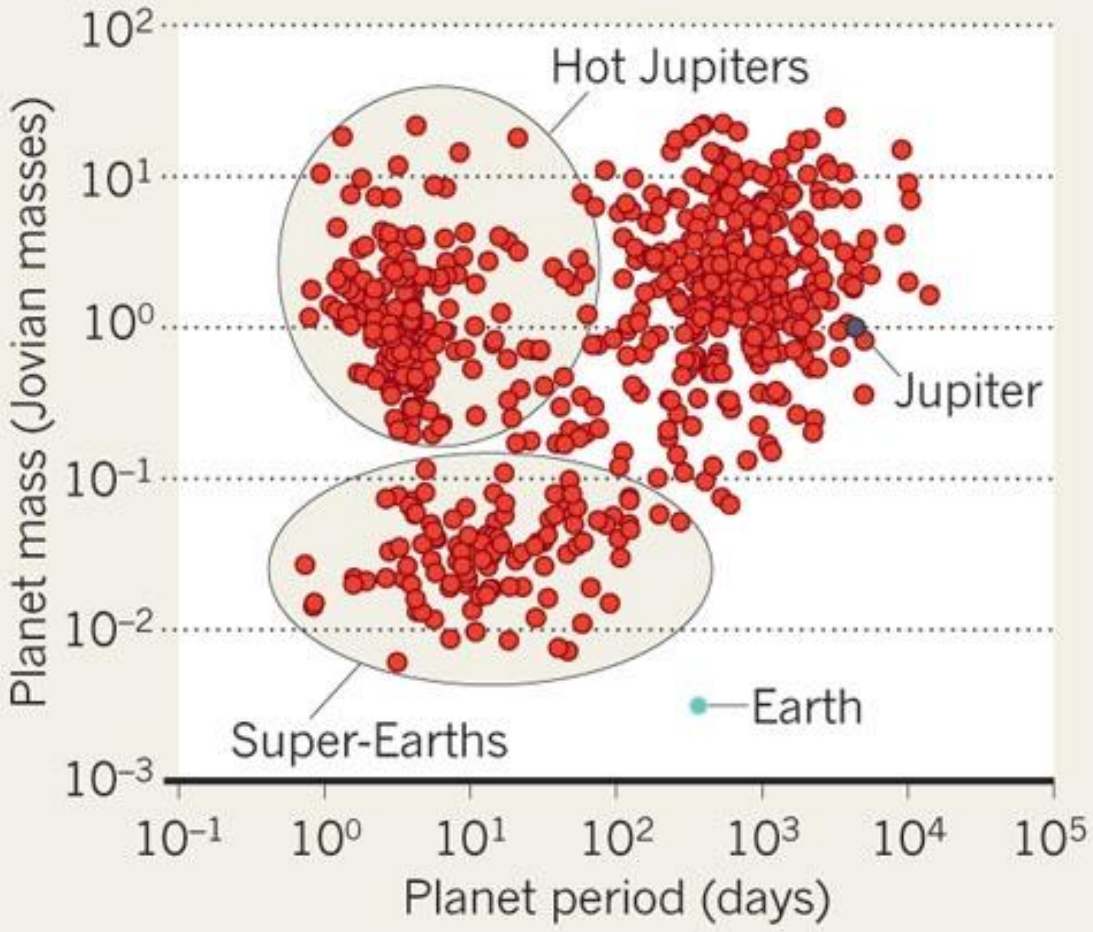

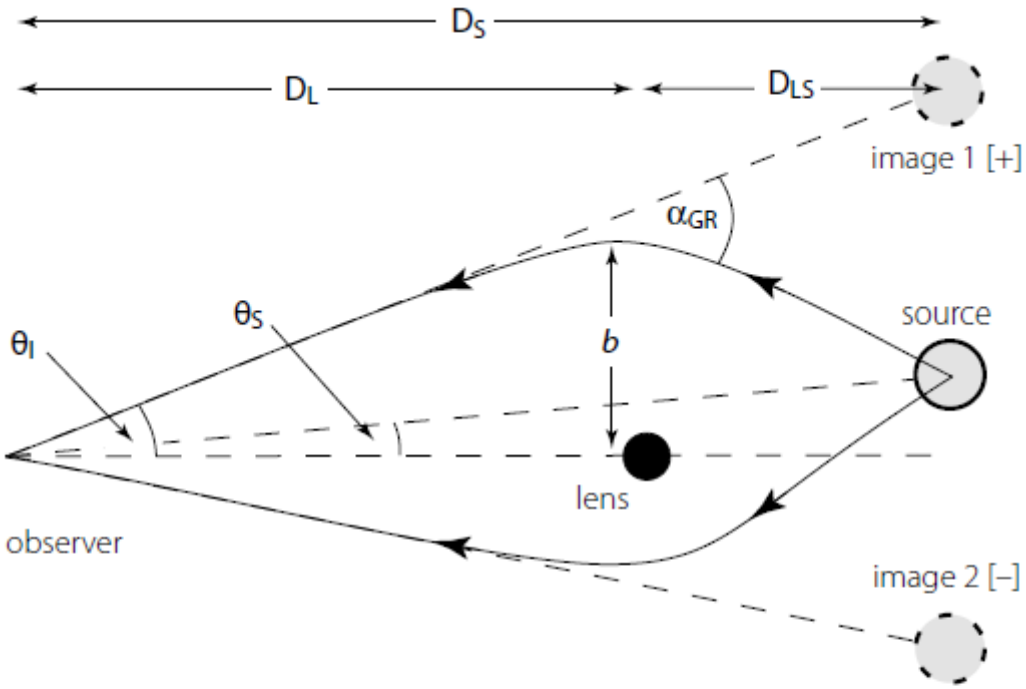

Figure 5.1: Lensing schematic for a point mass lens M_L at distance D_L, offset by the small angle θ_S from the direct line from observer to source. A light ray from the source, passing the lens at distance b, is deflected by an angle α_{GR}. An observer sees one image of the source displaced to angular position $\theta_I = b/D_L$ on the same side as the source, and a second image on the other.

The MACHO Project: Microlensing Results from 5.7 Years of LMC Observations

The MACHO collaboration: C. Alcock, R.A. Allsman, D.R. Alves, T.S. Axelrod, A.C. Becker, D.P. Bennett, K.H. Cook, N. Dalal, A.J. Drake, K.C. Freeman, M. Geha, K. Griest, M.J. Lehner, S.L. Marshall, D. Minniti, C.A. Nelson, B.A. Peterson, P. Popowski, M.R. Pratt, P.J. Quinn, C.W. Stubbs, W. Sutherland, A.B. Tomaney, T. Vandehei, D. Welch

(Submitted on 15 Jan 2000)

We report on our search for microlensing towards the Large Magellanic Cloud (LMC). Analysis of 5.7 years of photometry on 11.9 million stars in the LMC reveals 13 - 17 microlensing events. This is significantly more than the $\sim$ 2 to 4 events expected from lensing by known stellar populations. The timescales ($\that$) of the events range from 34 to 230 days. We estimate the microlensing optical depth towards the LMC from events with $2 < \that < 400$ days to be 1.2 ^{+0.4}_

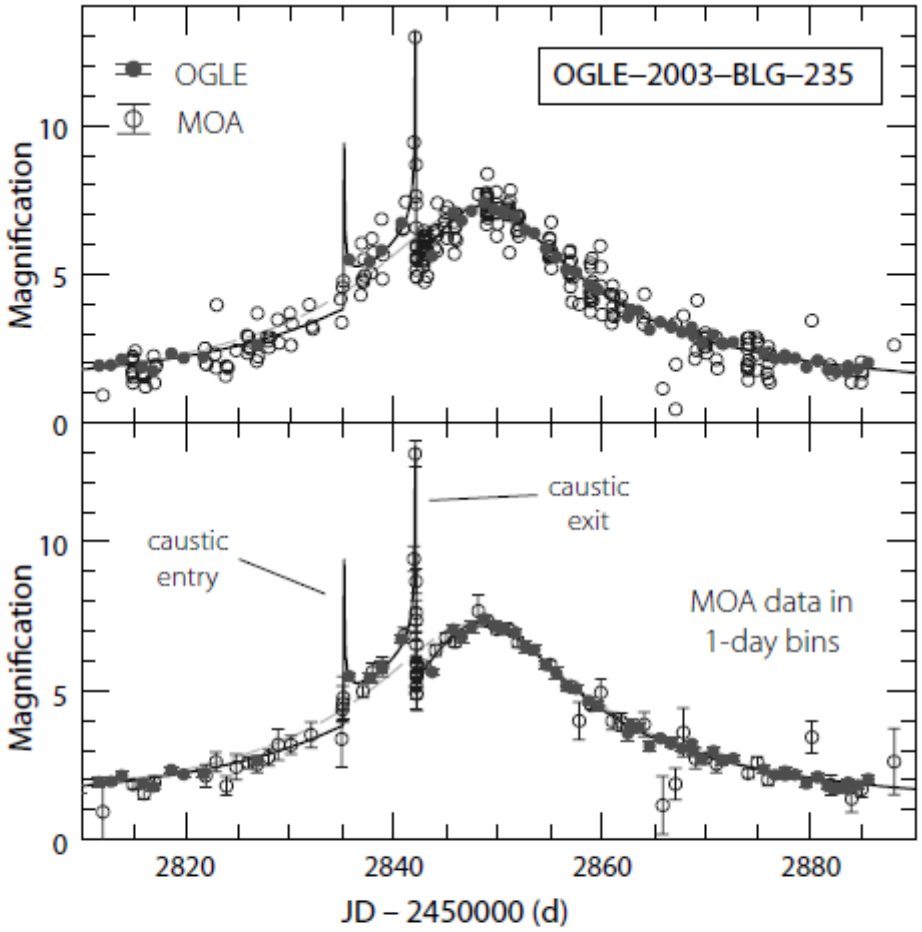

Figure 5.14: The first microlensing planet system, OGLE–2003–BLG–235, with data from OGLE and MOA over a period of about 80 days during 2003. The bottom panel shows binned data. Caustic crossings (entry and exit) occur on days 2835 and 2842. The binary and single lens fits are shown by the solid and fainter (lower) lines respectively. From Bond et al. (2004, Figure 1), reproduced by permission of the AAS.

Free-Floating Planets May be More Common Than Stars

This artist's conception illustrates a Jupiter-like planet alone in the dark of space, floating freely without a parent star. Astronomers recently uncovered evidence for 10 such lone worlds, thought to have been "booted," or ejected, from developing solar systems. Image credit: NASA/JPL-Caltech › Full image and caption | › See animation

May 18, 2011

PASADENA, Calif. -- Astronomers, including a NASA-funded team member, have discovered a new class of Jupiter-sized planets floating alone in the dark of space, away from the light of a star. The team believes these lone worlds were probably ejected from developing planetary systems.

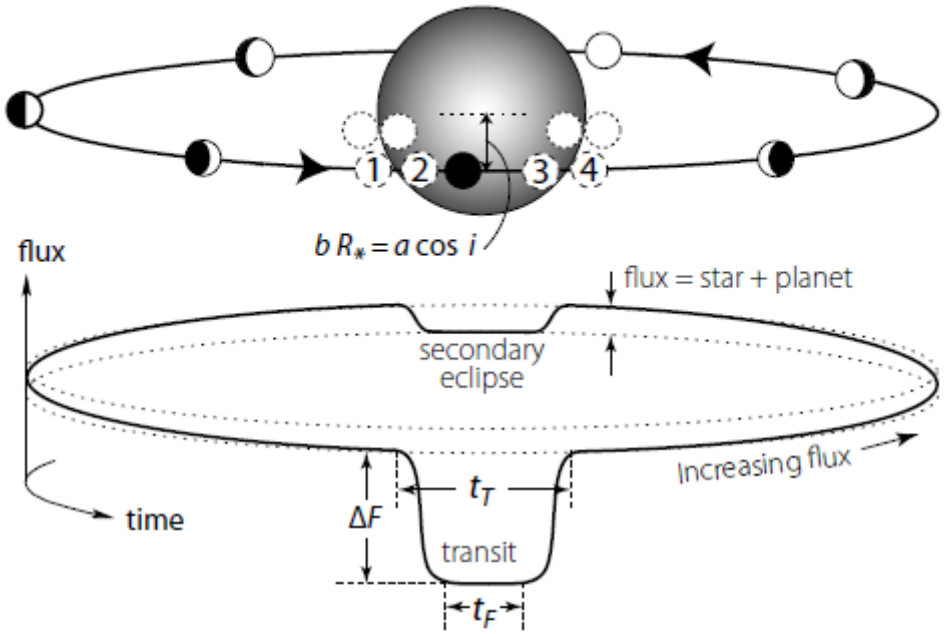

Figure 6.9: Schematic of a transit. During the transit, the planet blocks a fraction of the star light. After the transit, the planet's brighter day-side progressively comes into view, and the total flux rises. It drops again during the secondary eclipse as the planet passes behind the star. Dashed circles show the first to fourth contact points; those for smaller impact parameter (dotted) are more closely separated in time, and the ingress/egress slopes correspondingly steeper. The total transit duration t_T is between first and fourth contact, while t_F is timed between second and third contact. After Winn (2009, Figure 1).

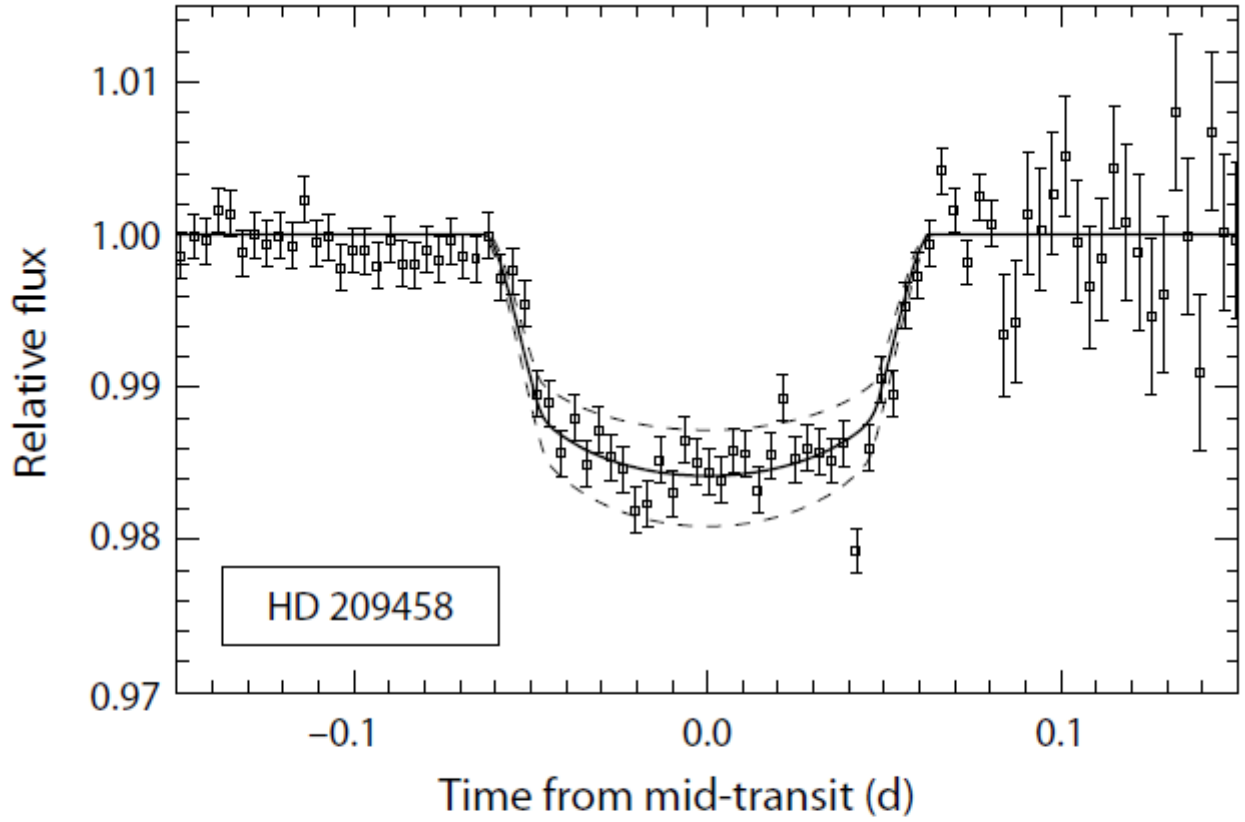

Figure 6.1: The first detected transiting exoplanet, HD 209458, showing the measured flux versus time. Measurement noise increases to the right due to increasing atmospheric air mass. From Charbonneau et al. (2000, Figure 2), reproduced by permission of the AAS.

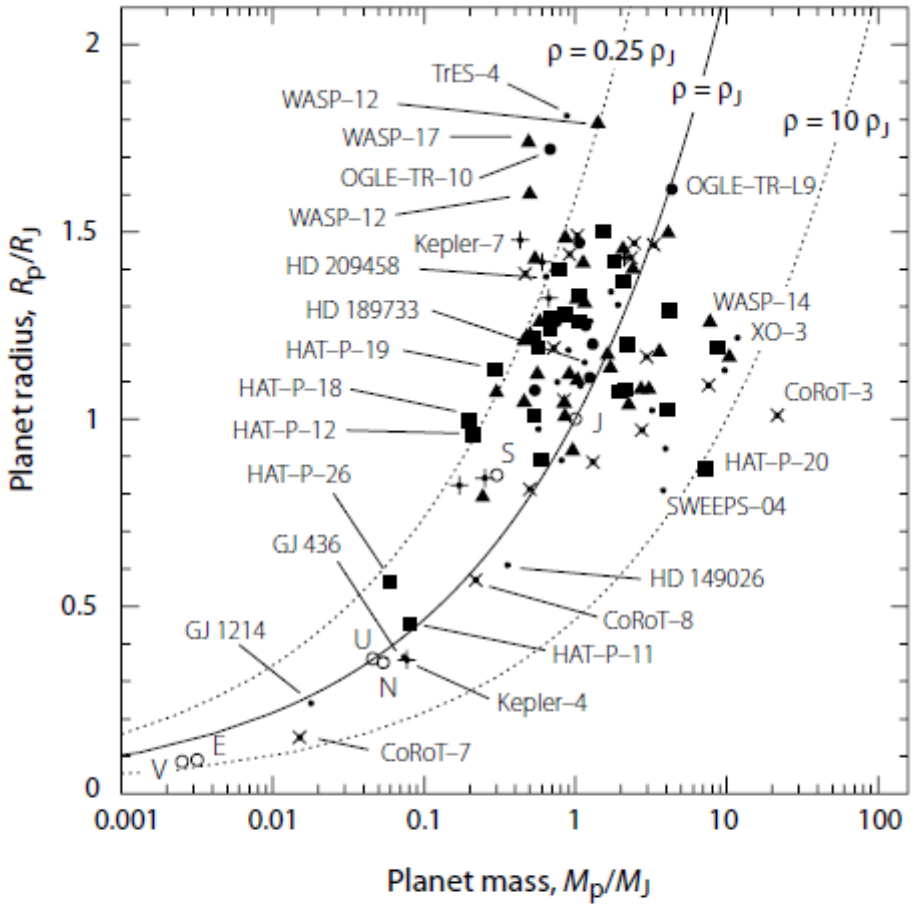

Figure 6.33: Mass–radius diagram for transiting exoplanets (● OGLE, ▲ WASP, ■ HAT, × CoRoT, + Kepler, · other). Data are from `exoplanet.eu`*, 2010 November 1 (Appendix D).* V, E, J, S, U, N *indicate positions of Venus, Earth, Jupiter, Saturn, Uranus, Neptune. Dashed lines are of constant density in Jovian units* $(0.25, 1, 10\rho_J)$*. CoRoT–3 b* $(22 M_J)$ *is a brown dwarf.*

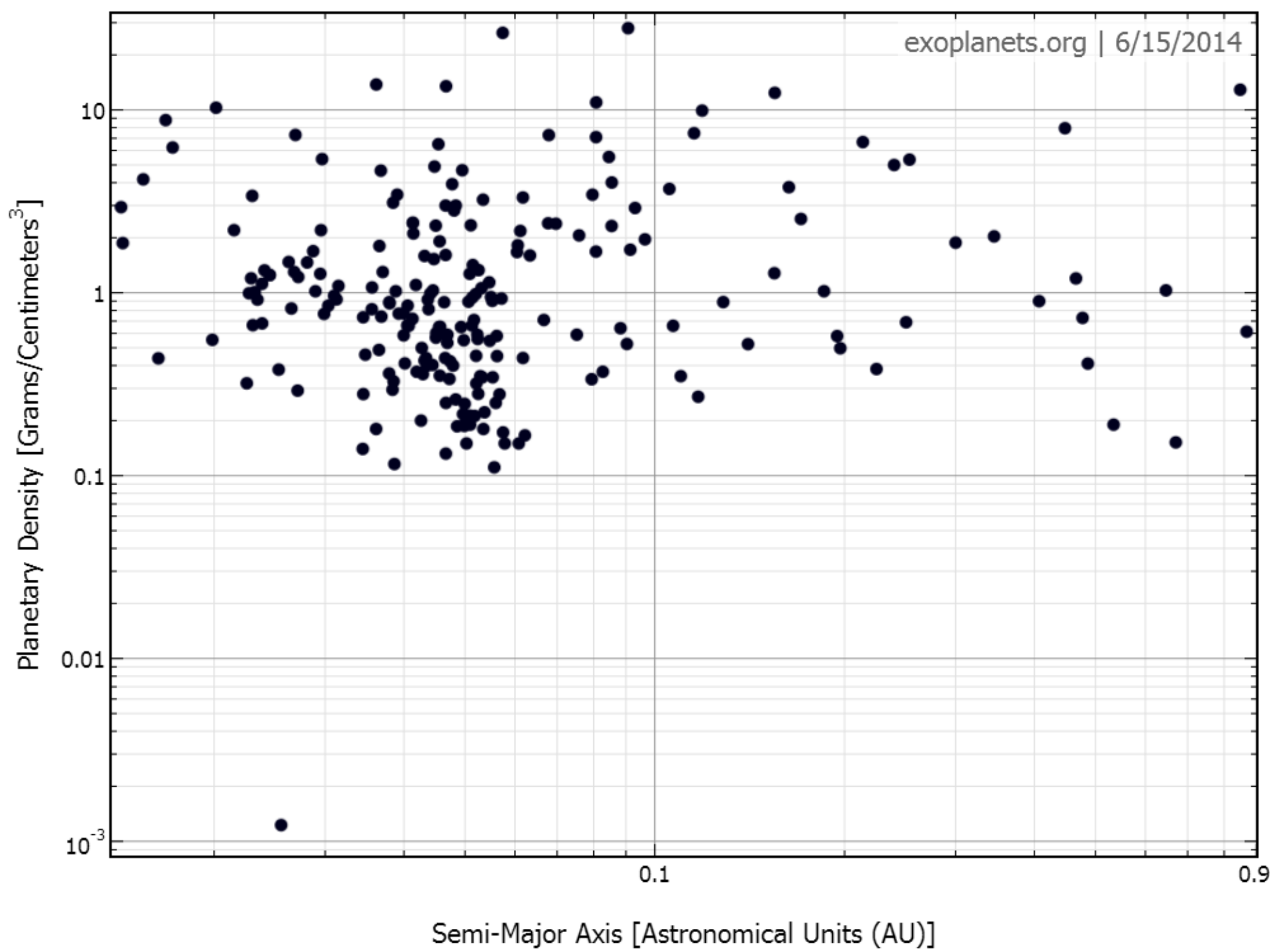
exoplanets.org | 6/15/2014
Planetary Density [Grams/Centimeters^3]
10
1
0.1
0.01
10^{-3}
0.1
0.9
Semi-Major Axis [Astronomical Units (AU)]

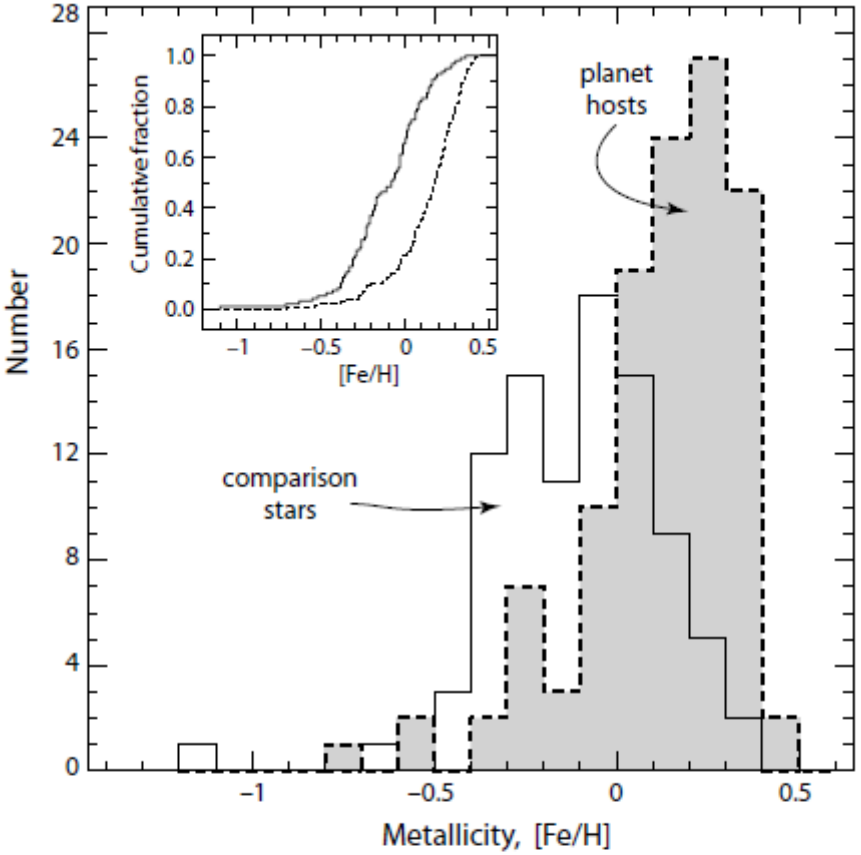

Figure 8.7: Metallicity distribution for 119 planet-host stars (shown as the dashed line, shaded), and for a volume-limited comparison sample of 94 stars with no known planets (continuous line, unshaded). The average metallicity difference of the two samples is 0.24 dex. Inset: cumulative distribution functions. A statistical Kolmogorov–Smirnov test shows that the probability that both distributions belong to the same population is $\sim 10^{-12}$. *From Santos et al. (2005, Figure 1), reproduced with permission © ESO.*

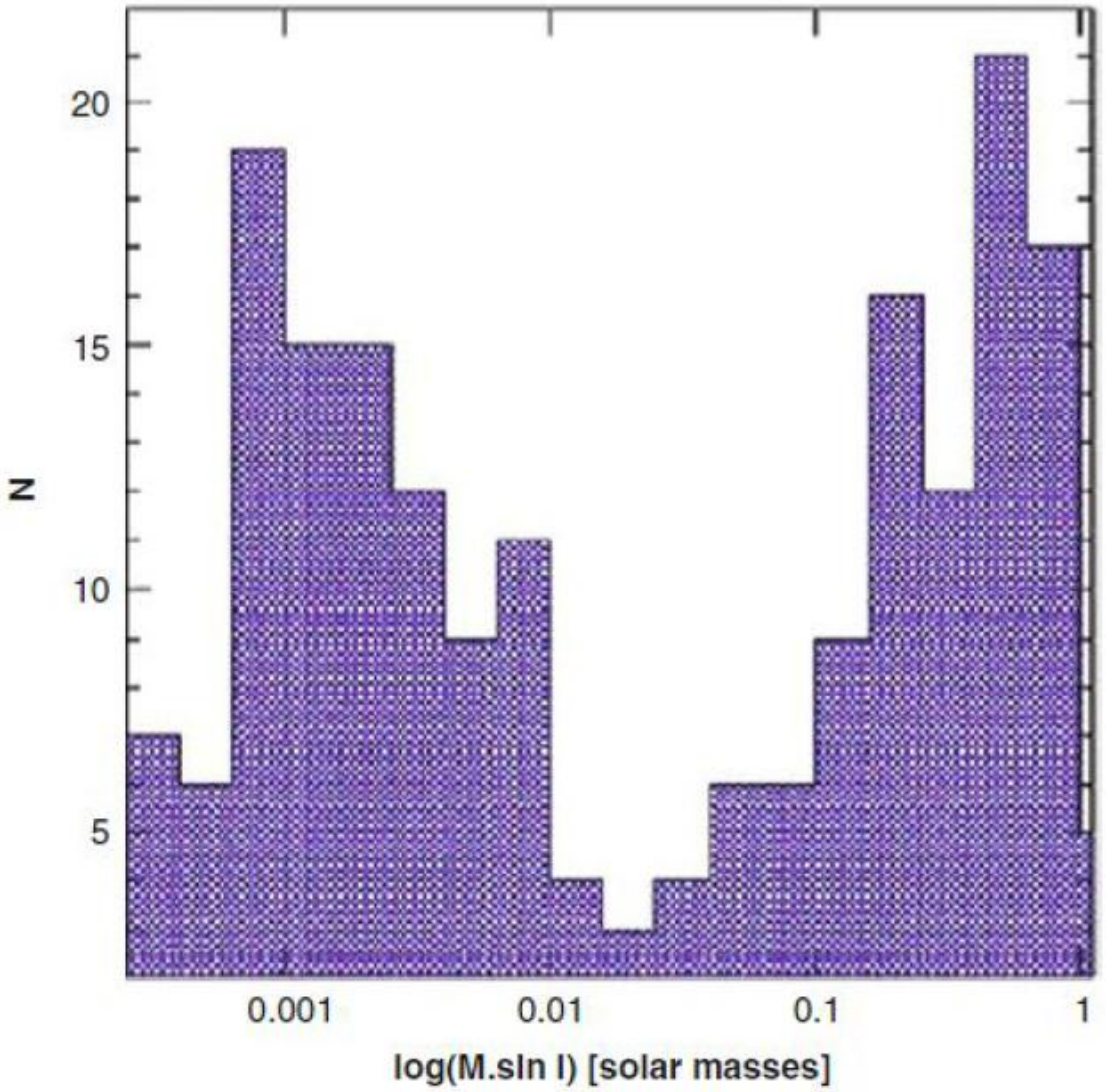

Fig. 3.2 Histogram of the mass-distribution – more precisely, $M.sin(i)$ - for the stellar and sub-stellar companions discovered by the radial-velocity method. It is obvious that the distribution is bimodal with planets on the left, and stars on the right. The poorly populated central zone between the two peaks (where $0.01\ M_{\odot} < M.sin(i) < 0.08\ M_{\odot}$) is known as the 'brown dwarf desert' (After Santos et al. (2002))

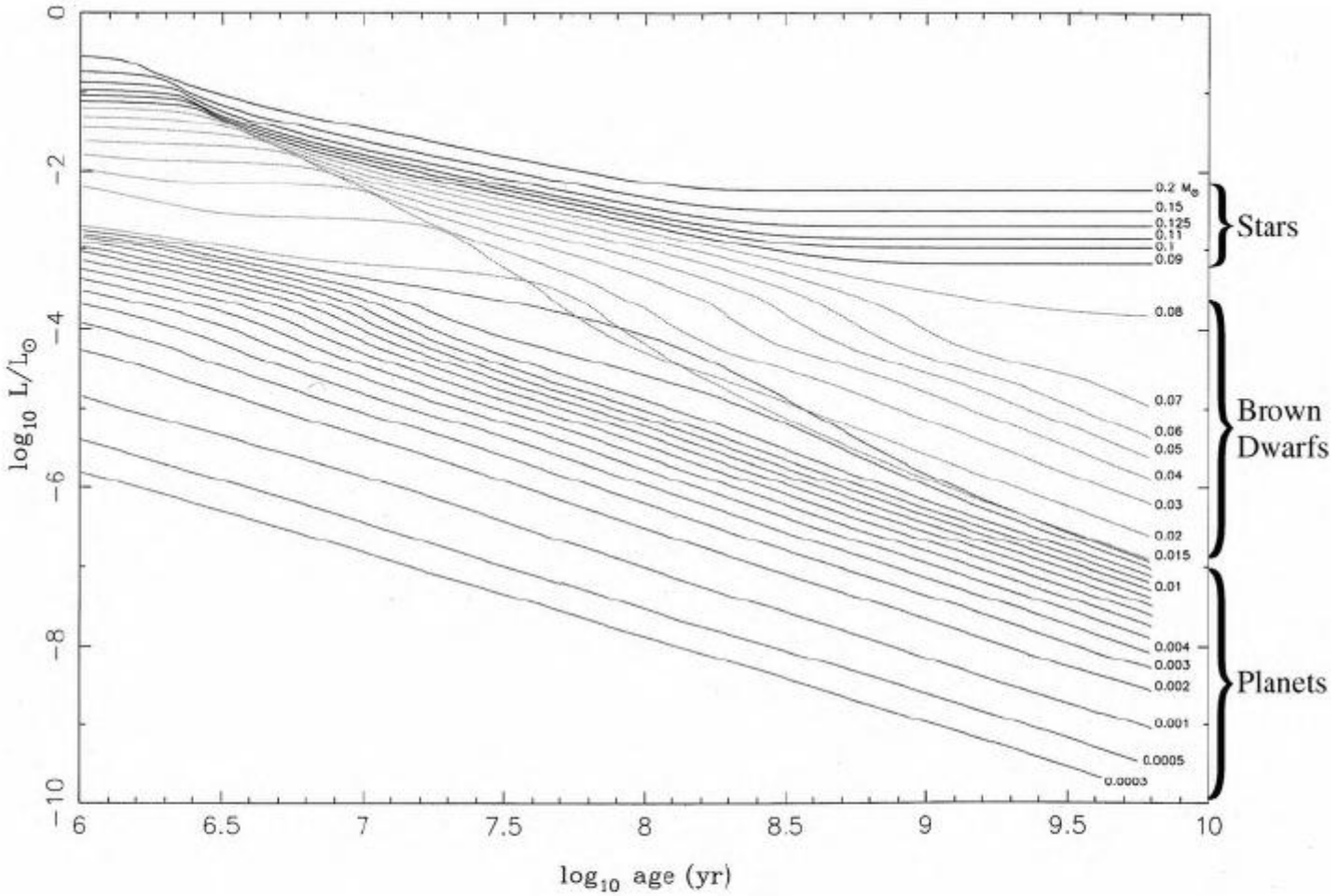

Figure 3.7 Evolution of the luminosity (in $\mathcal{L}_\odot$) of initially hot and distended very low mass stars and substellar objects plotted as functions of time (in years) after formation. All of these objects are isolated and have solar-metallicity. The stars, brown dwarfs and planets are shown as the upper, middle and lower sets of curves, respectively. The curves are labeled by the object's mass in units of $M_\odot$; the lowest curve corresponds to the mass of Saturn. All of the substellar objects become less luminous as they radiate away the energy released by their gravitational contraction from large objects to much more compact bodies with sizes of order $R_\clubsuit$. Stars ultimately level off in luminosity when they reach the hydrogen burning main sequence. In contrast, the luminosities of brown dwarfs and planets decline indefinitely. Objects with $M \gtrsim 0.012\ M_\odot$ exhibit plateaus between 10^6 and 10^8 years as a result of deuterium burning. The luminosities of the younger objects, especially giant planets $\lesssim 10^8$ years old, may be substantially smaller than the values shown here if they radiate away substantial portions of their accretion energy while they are growing. (Burrows et al. 1997)

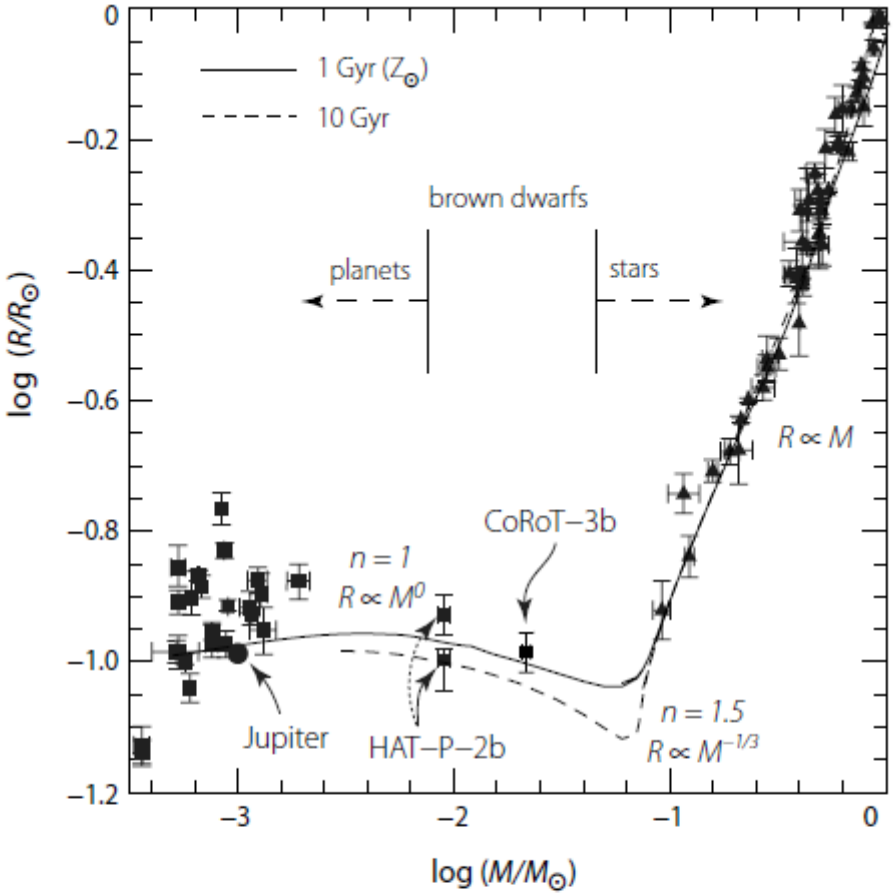

Figure 6.34: Mass–radius relation for stars and planets. Solid and short-dashed lines are models with solar composition for two isochrones, and n indicates the relevant polytropic index. Lines demarcating planets and stars are somewhat arbitrary. The CoRoT–3 b radius is from Deleuil et al. (2008). For HAT–P–2 b, both the original determination (lower point, Bakos et al., 2007a) and a later revision (upper point, Pál et al., 2010) are shown. From Chabrier et al. (2009, Figure 2).

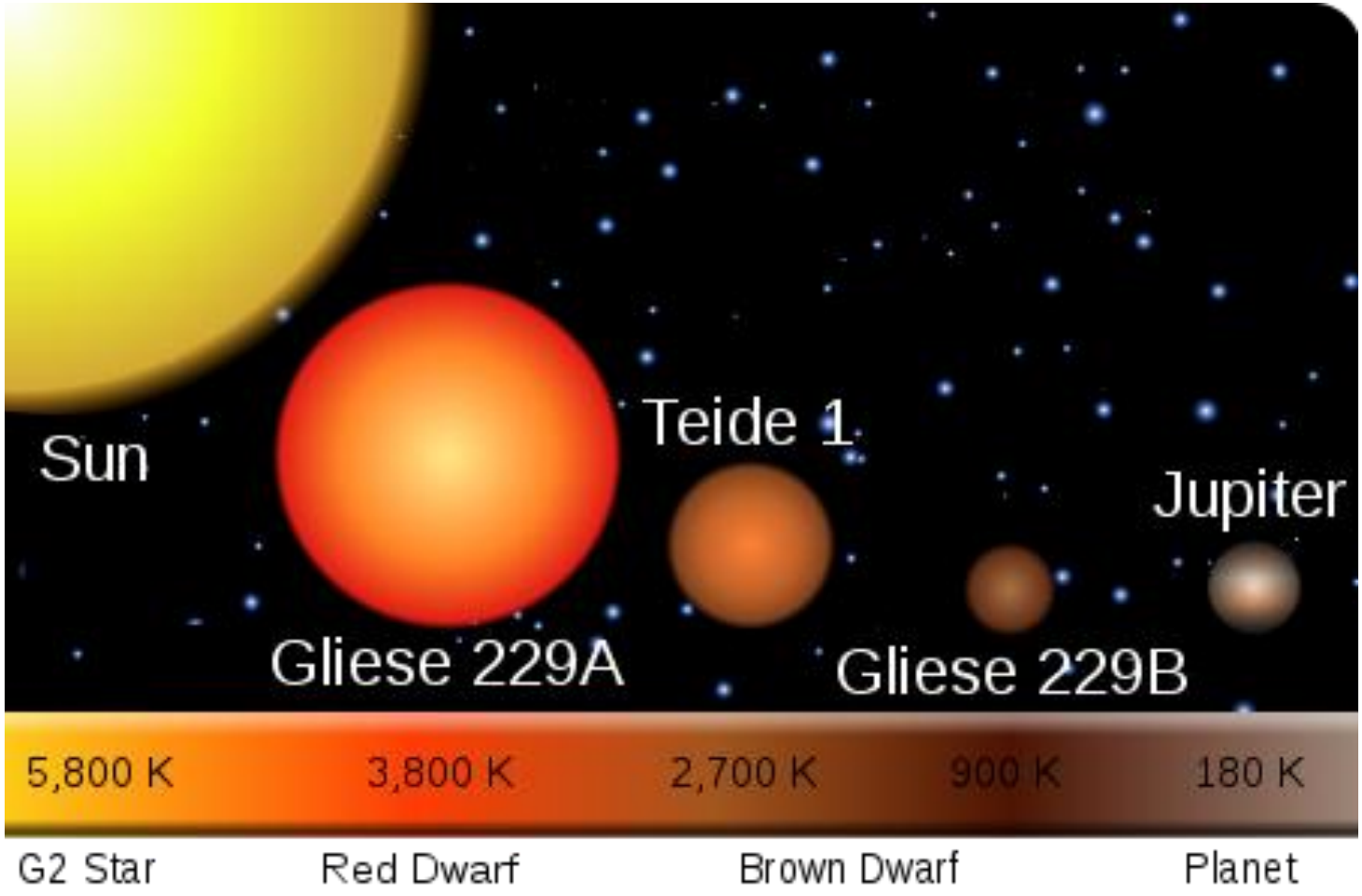
Sun
Gliese 229A
Teide 1
Gliese 229B
Jupiter
5,800 K
3,800 K
2,700 K
900 K
180 K
G2 Star
Red Dwarf
Brown Dwarf
Planet

Tabare Gallardo, Dpto. Astronomia, Facultad de Ciencias

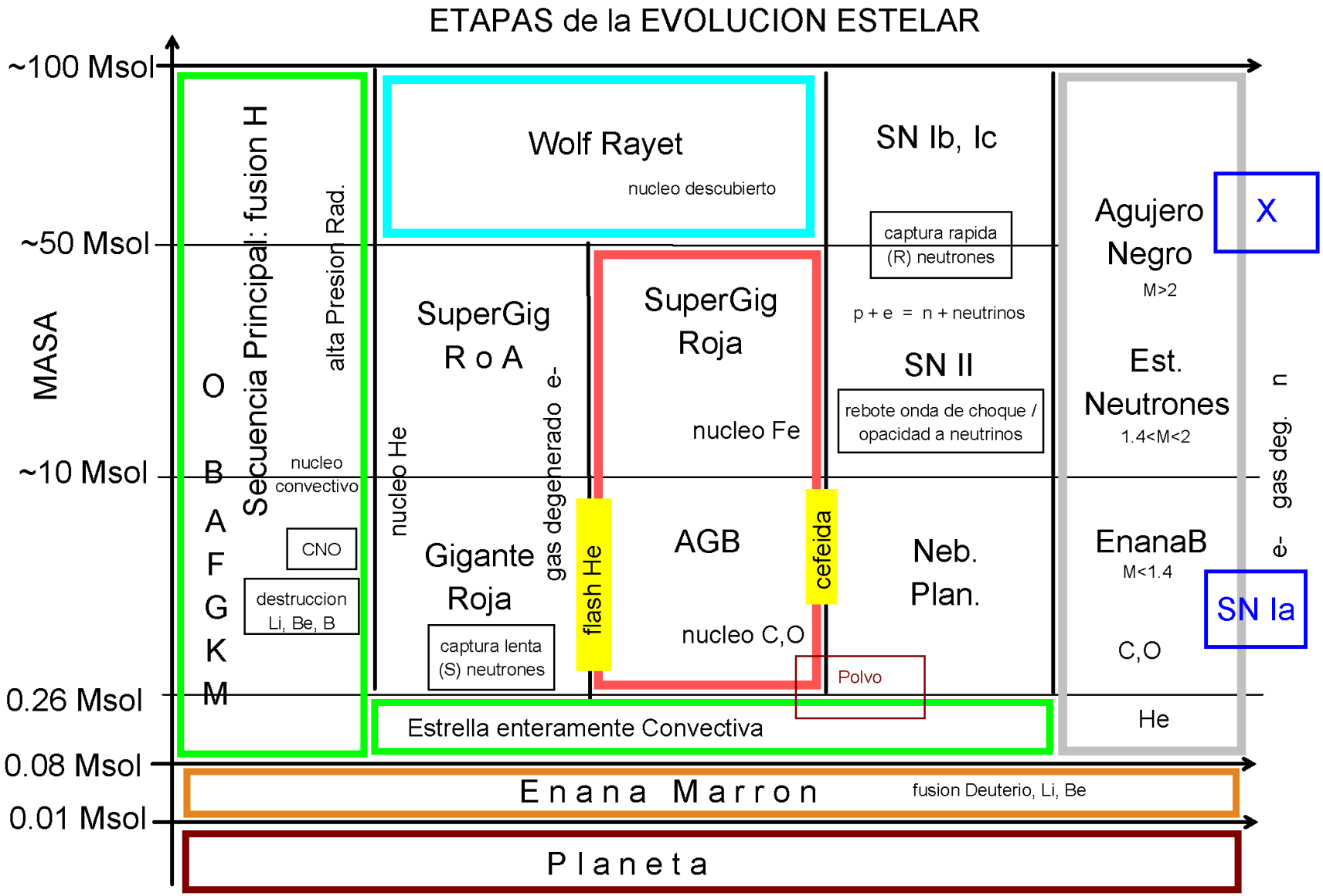

FORMACION PLANETARIA

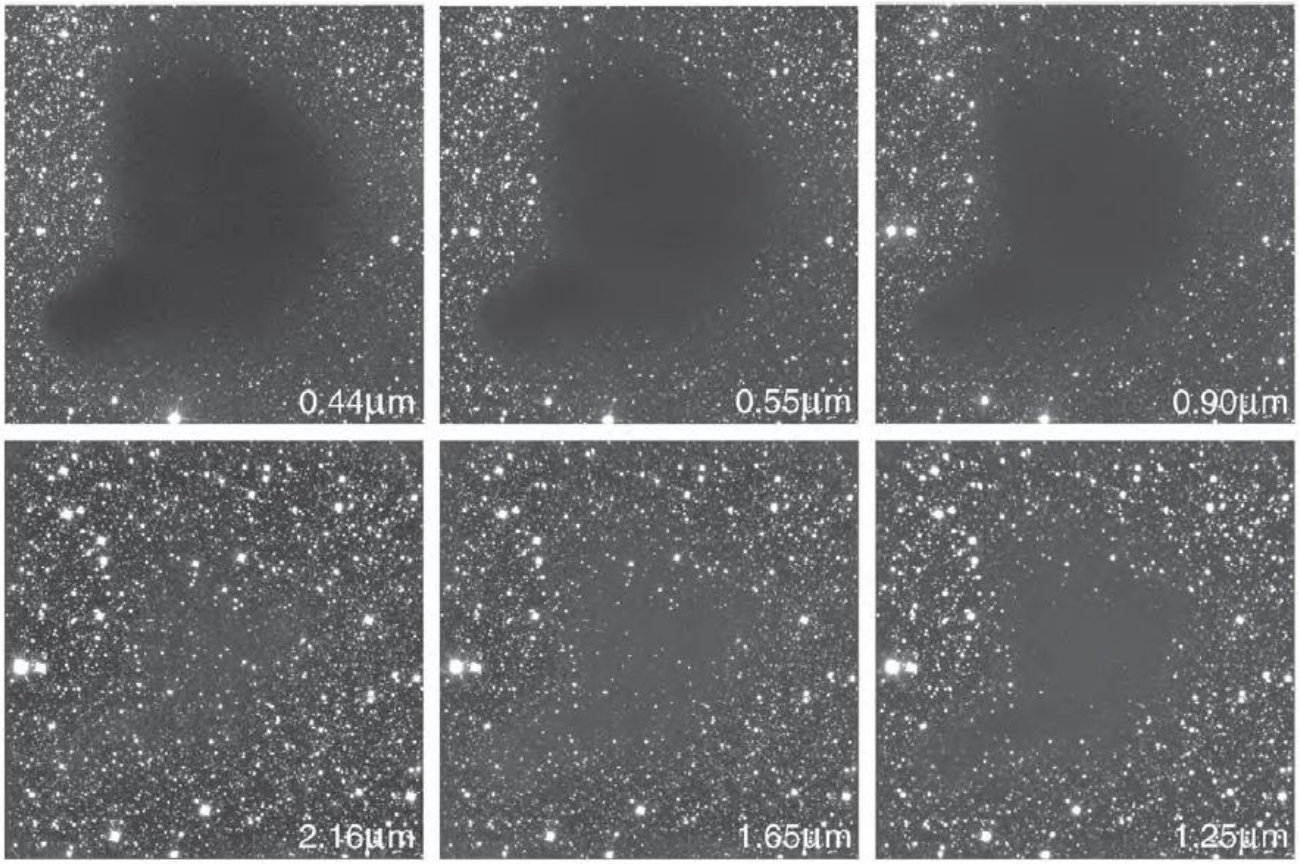

Figure 15.1 The sky area of the globule Barnard 68 in the Ophiuchus star-forming region, imaged in six different wavebands, clockwise from the blue to the near-infrared spectral region. The obscuration caused by the cloud diminishes dramatically with increasing wavelength, implying that most of the dust is in the form of sub-μm grains. Because the outer regions of the cloud are less dense than the inner ones, the apparent size of the cloud also decreases as wavelength increases, with more background stars shining through the outer parts. (European Southern Observatory PR Photo 29b/99)

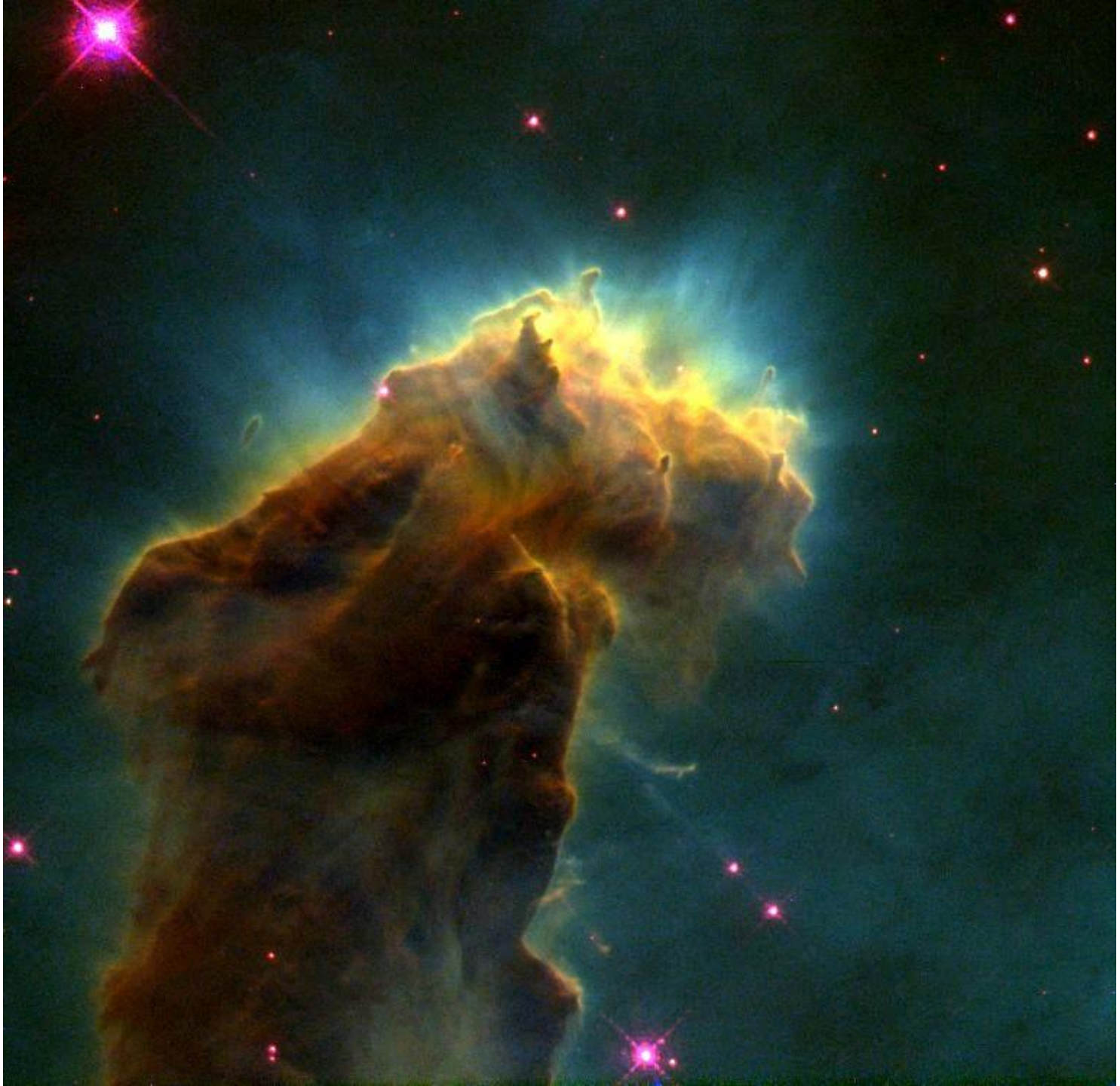

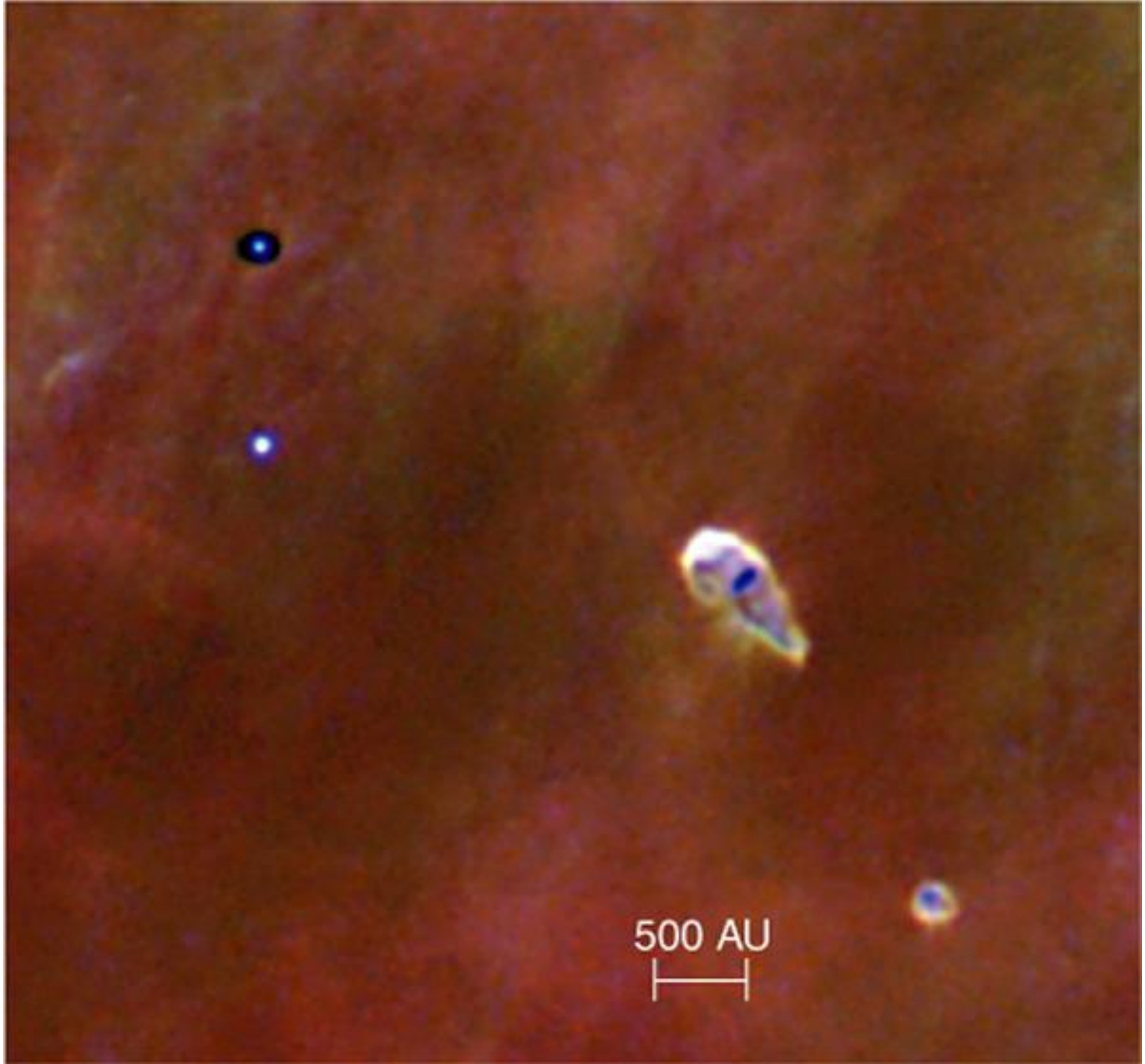
500 AU

Fig. 5.3 A diagram illustrating star formation. The star forms following the collapse of a rotating cloud of interstellar material, which flattens into a disk, perpendicular to its rotation axis. The stellar wind, which is confined by the magnetic field, escapes in two lobes that are aligned with the rotation axis (After Acker, 2005)

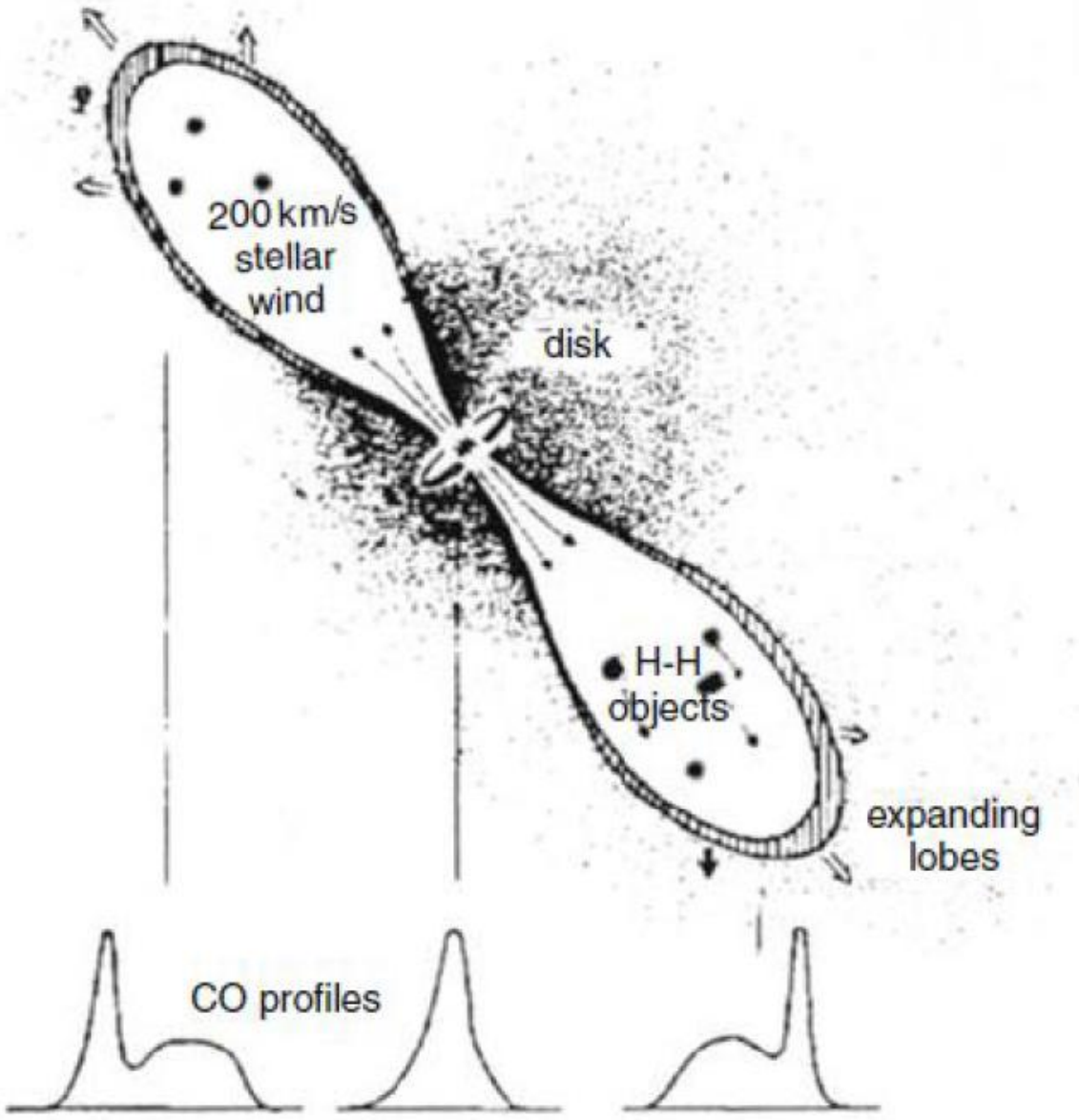

Snell 1980

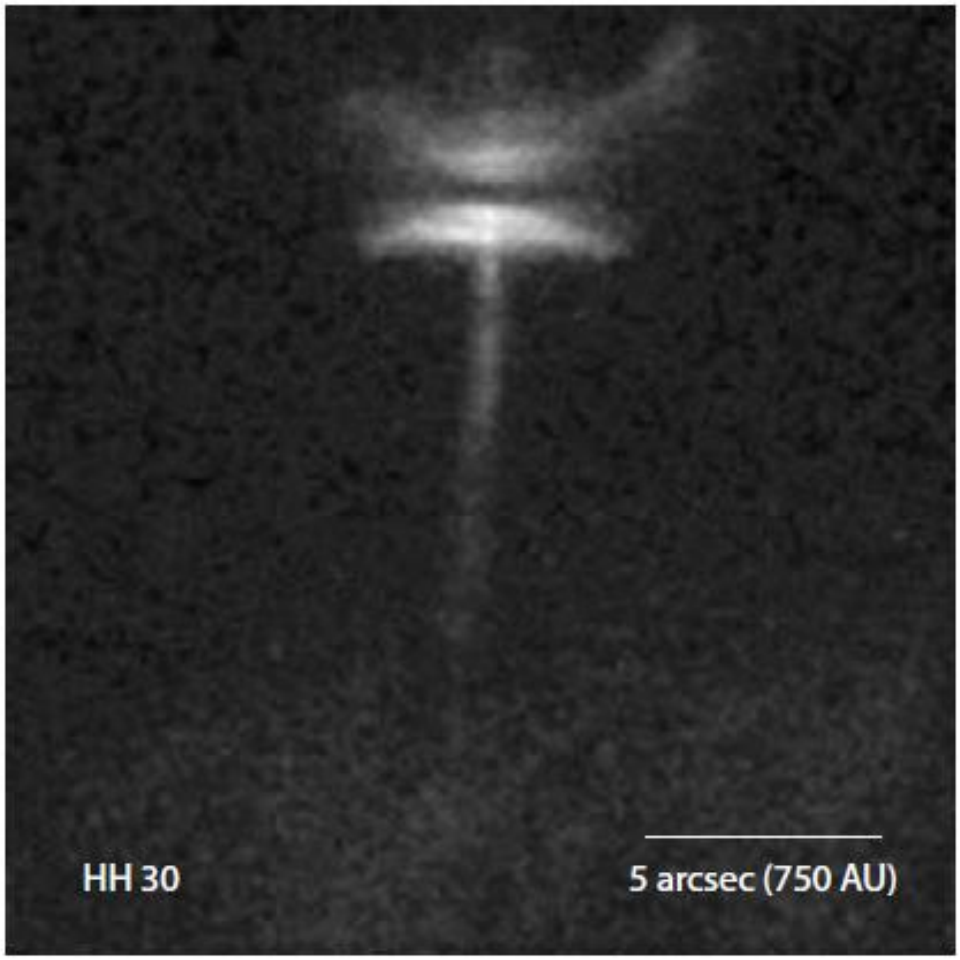

Figure 10.2: The Herbig–Haro object HH30, at a distance of ~150 pc, observed by HST. Two thin jets flow outwards from the young stellar object in the centre. The two lenticular regions are scattered light from dust in the disk. The dark central lane is the accretion disk observed edge-on (courtesy NASA/ESA/STScI).

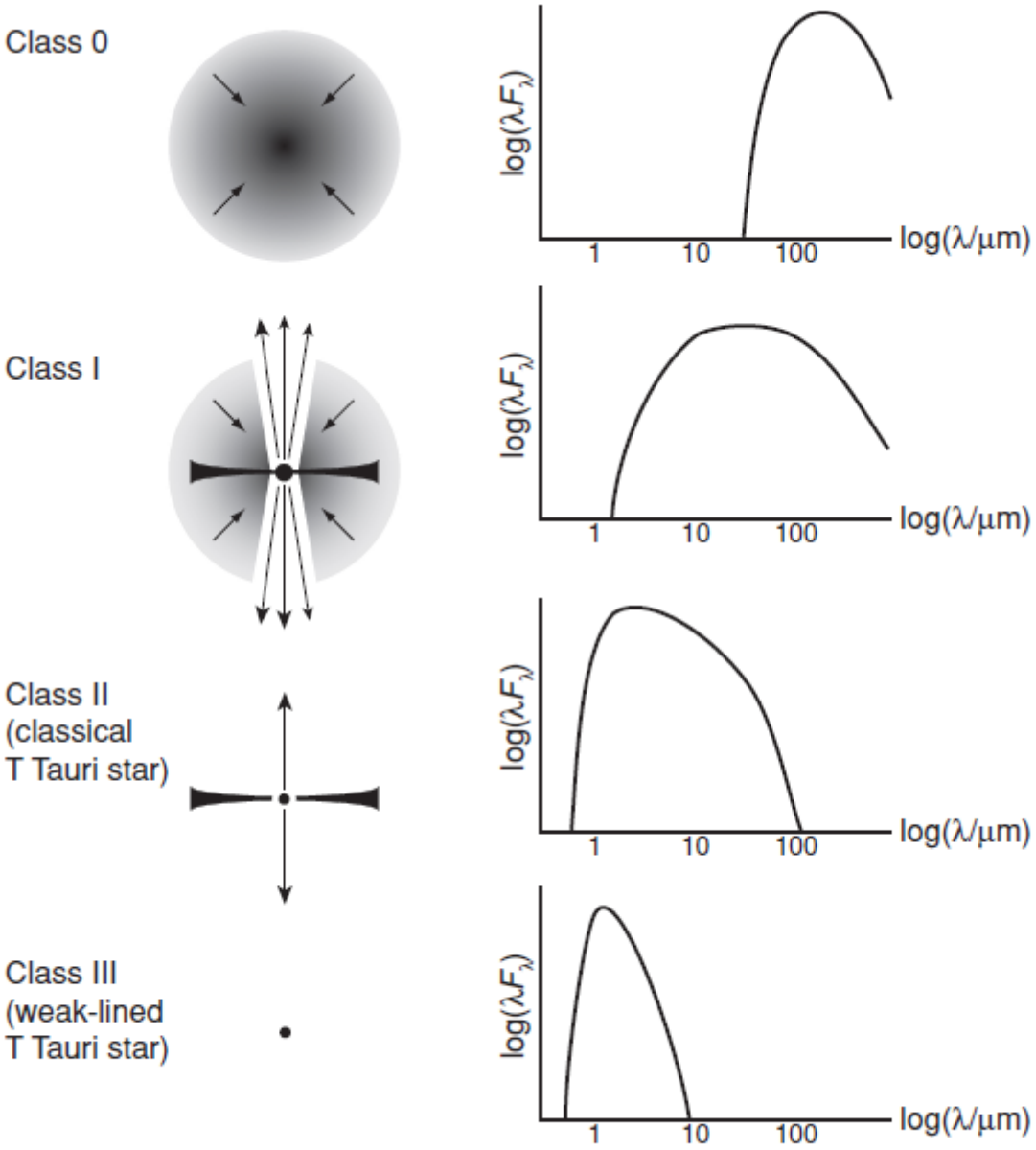

Fig. 2.1. Classification scheme for Young Stellar Objects.

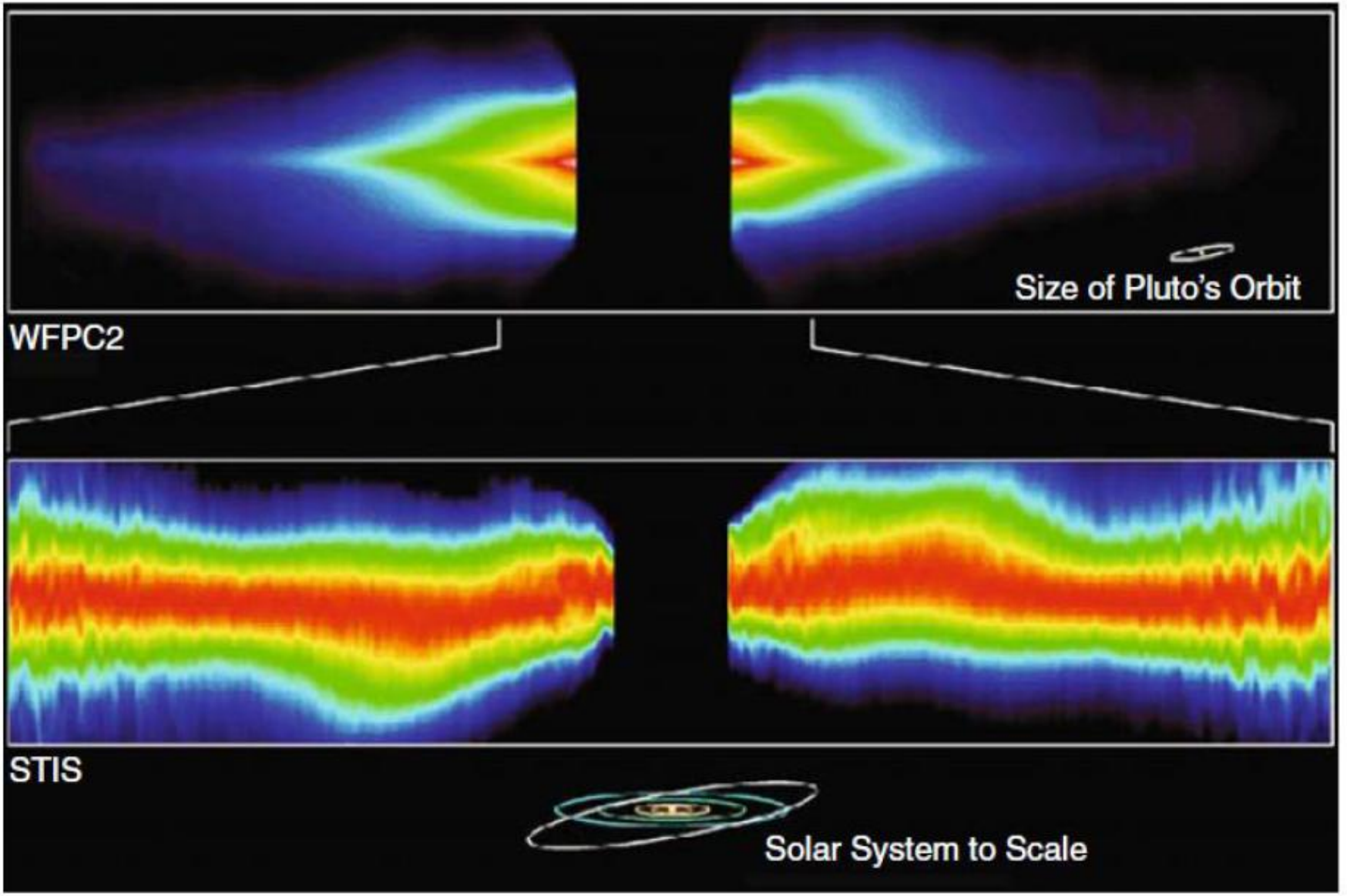

Fig. 5.22 Coronographic images of the disk of β Pic obtained with the STIS instrument on the HST. *Top*: overall image; *bottom*: enlargement of the central portion, with a vertical exaggeration of 4 times, to reveal the warping of the disk. The intensity (and thus the quantity of dust) is a maximum near the equatorial plane (After Heap et al., 2000)

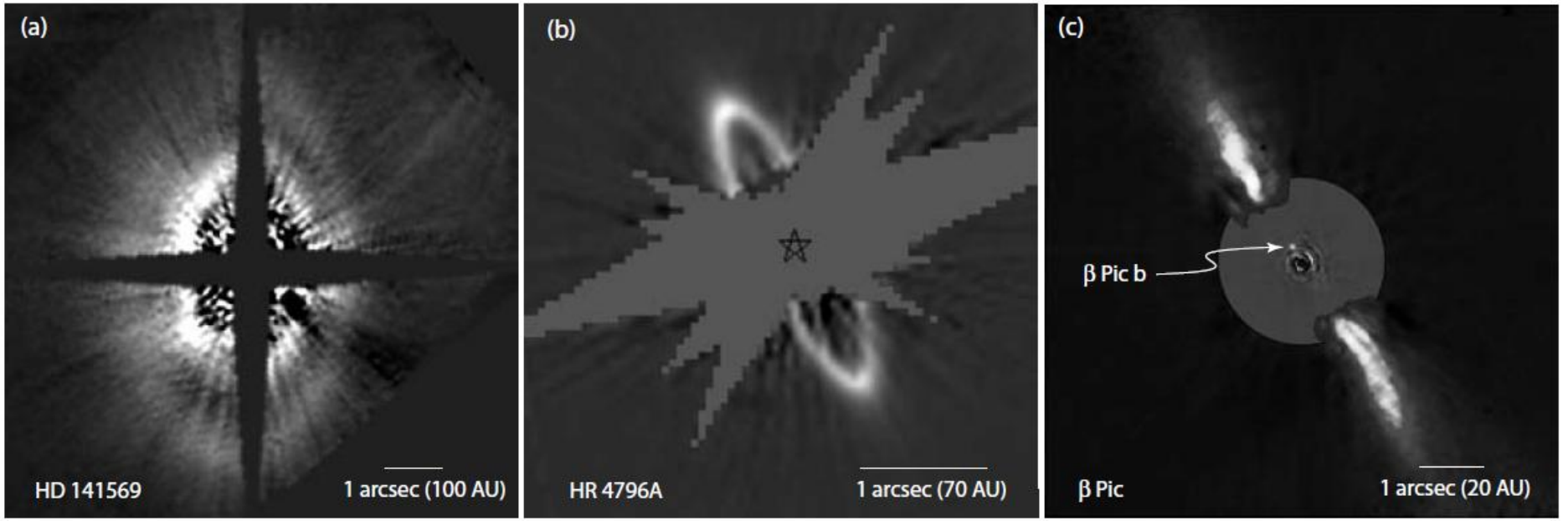

Figure 10.4: Examples of imaged debris disks: (a) HD 141569 observed at 1.1 μm with HST–NICMOS (Weinberger et al., 1999, Figure 1). (b) HR 4796A, observed in the optical with HST–STIS (Schneider et al., 2009a, Figure 2; this version courtesy G. Schneider). (c) β Pic, from combined ESO 3.6-m ADONIS imaging in 1996 (outer region), and 3.6 μm observations with VLT–NACO (inner region) revealing the probably planet, β Pic b (Lagrange et al., 2009b, this version courtesy A.M. Lagrange, D. Ehrenreich, and ESO). In all cases, the geometric central structures are artefacts of the coronagraphic imaging.

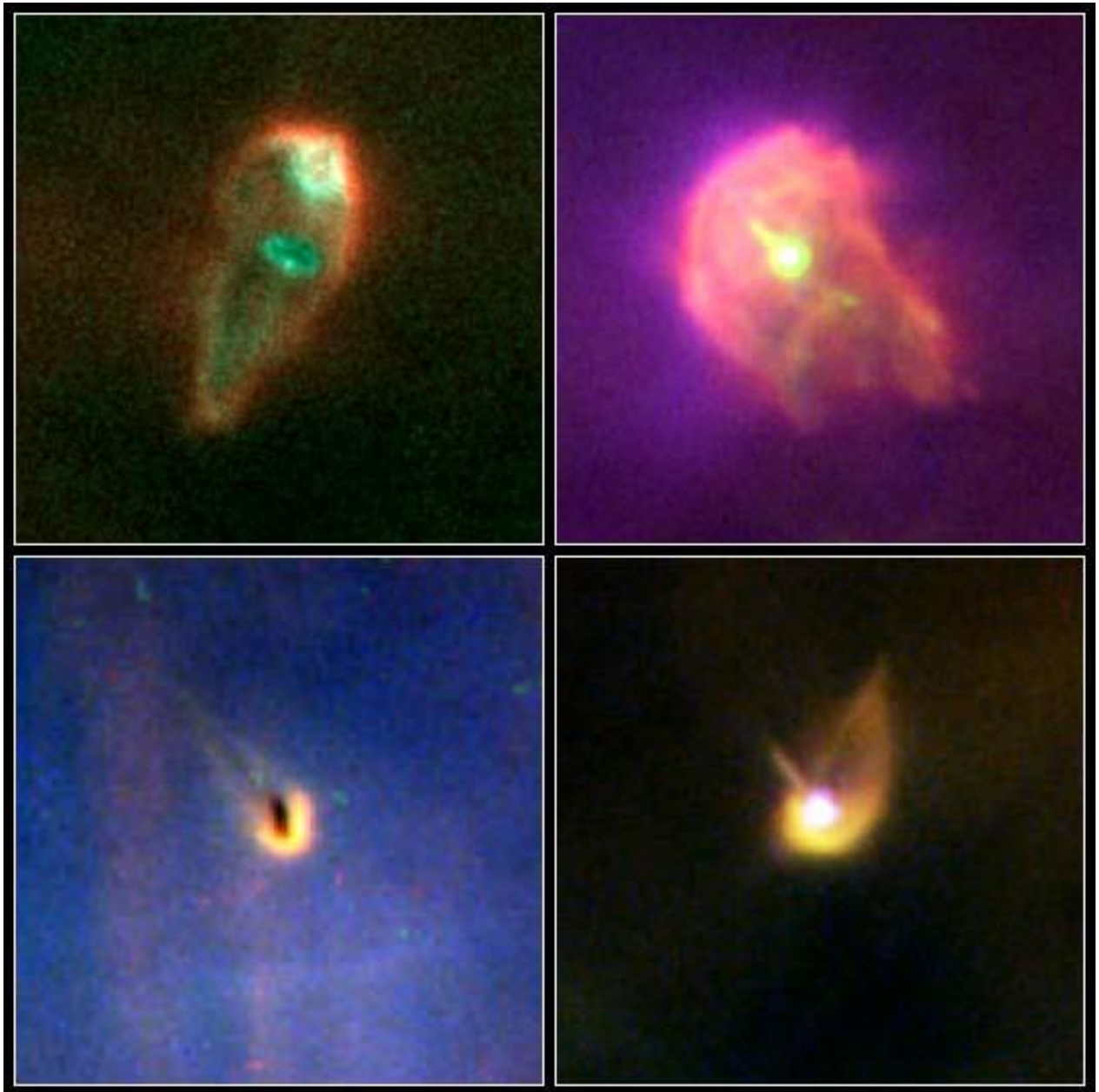

Protoplanetary Disks in the Orion Nebula **HST** • WFPC2

NASA, J. Bally (University of Colorado), H. Throop (SWRI),
and C.R. O'Dell (Vanderbilt University) • STScI-PRC01-13

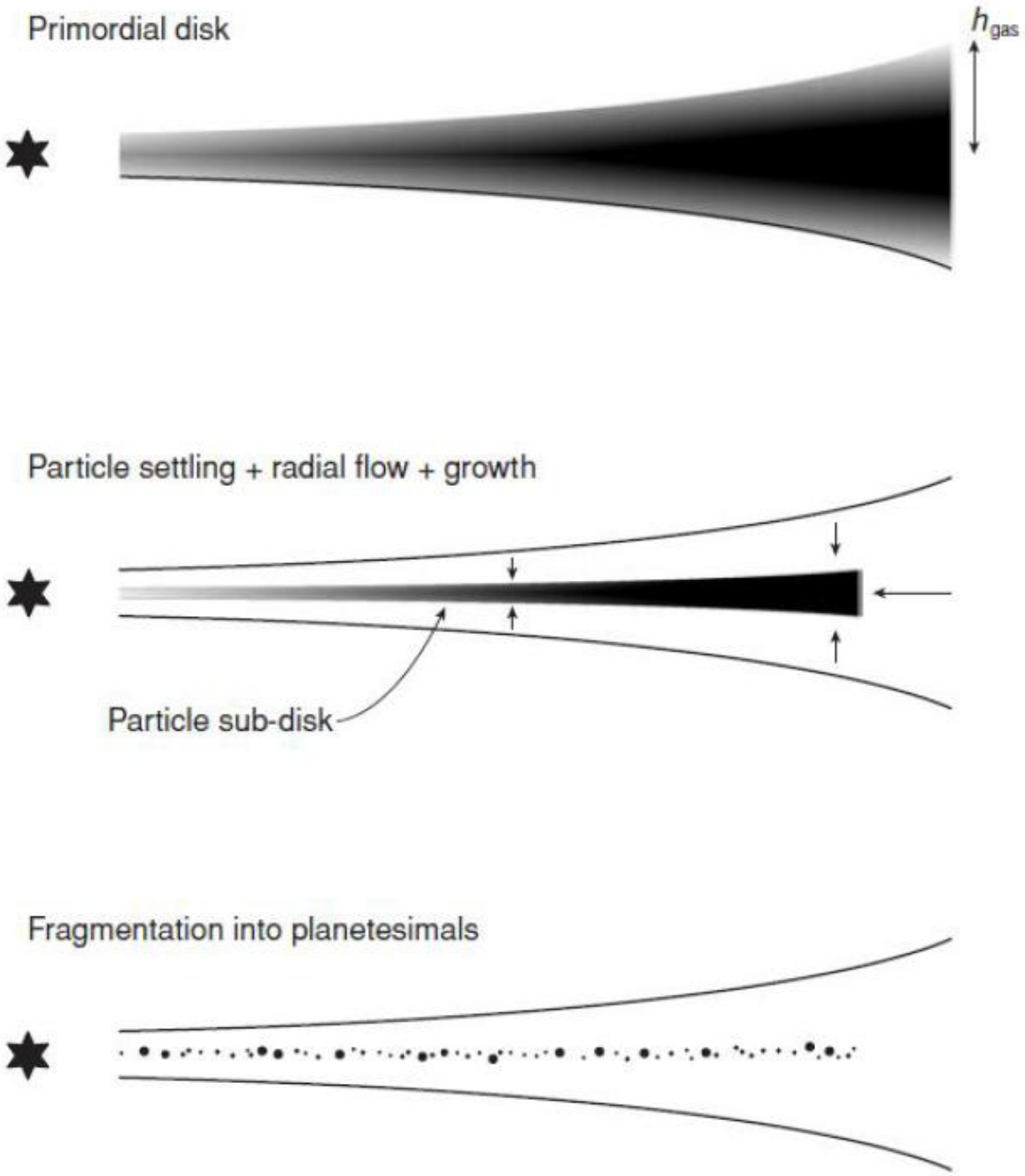

Fig. 4.7. How planetesimals form within the classical Goldreich–Ward scenario.

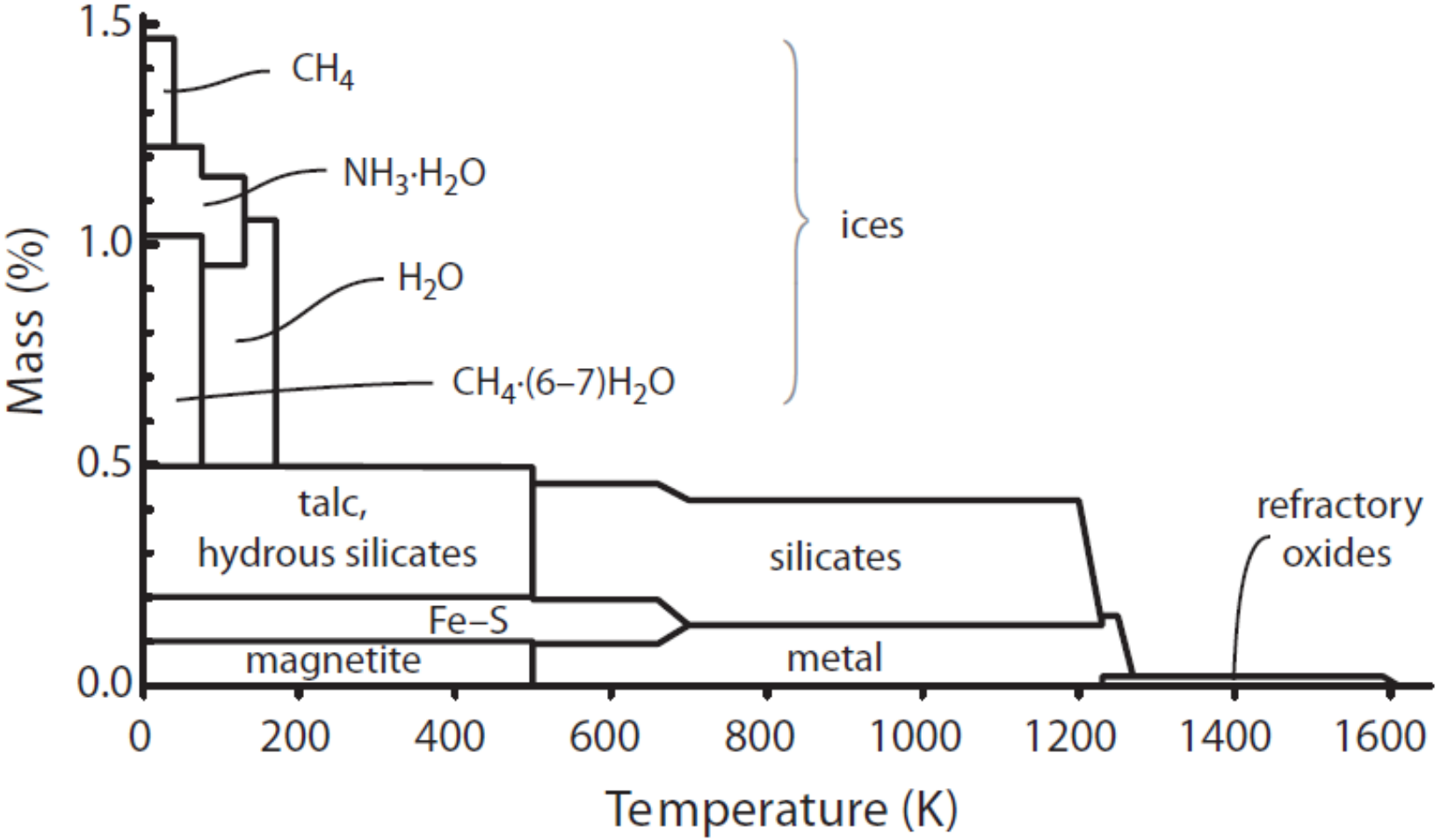

Figure 15.6 Amount and composition of major condensed components formed during fully equilibrated cooling of solar nebula material. (Lodders 2010)

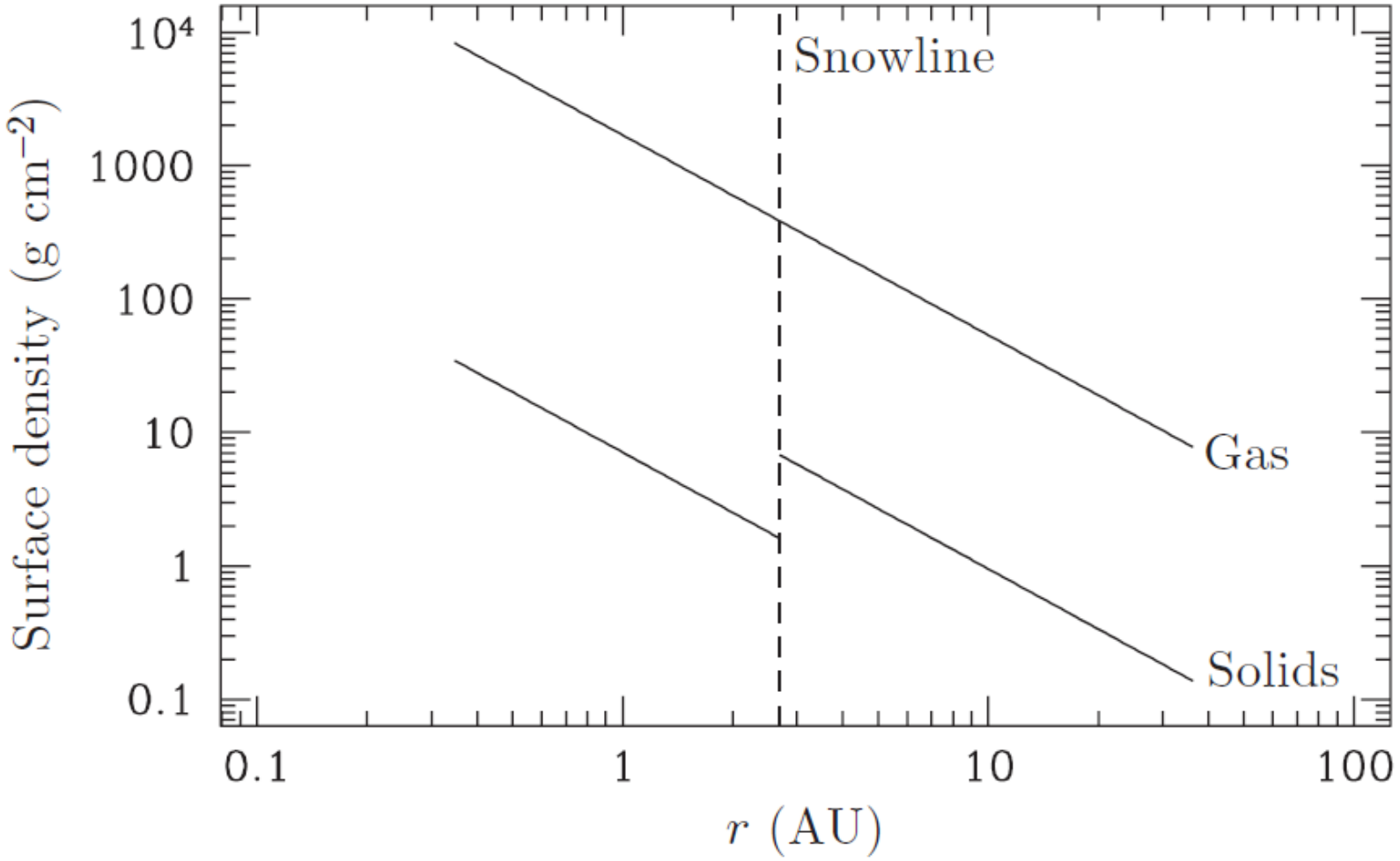

Fig. 1.1. The surface density in gas (upper line) and solids (lower broken line) as a function of radius in Hayashi's minimum mass Solar Nebula. The dashed vertical line denotes the location of the snowline.

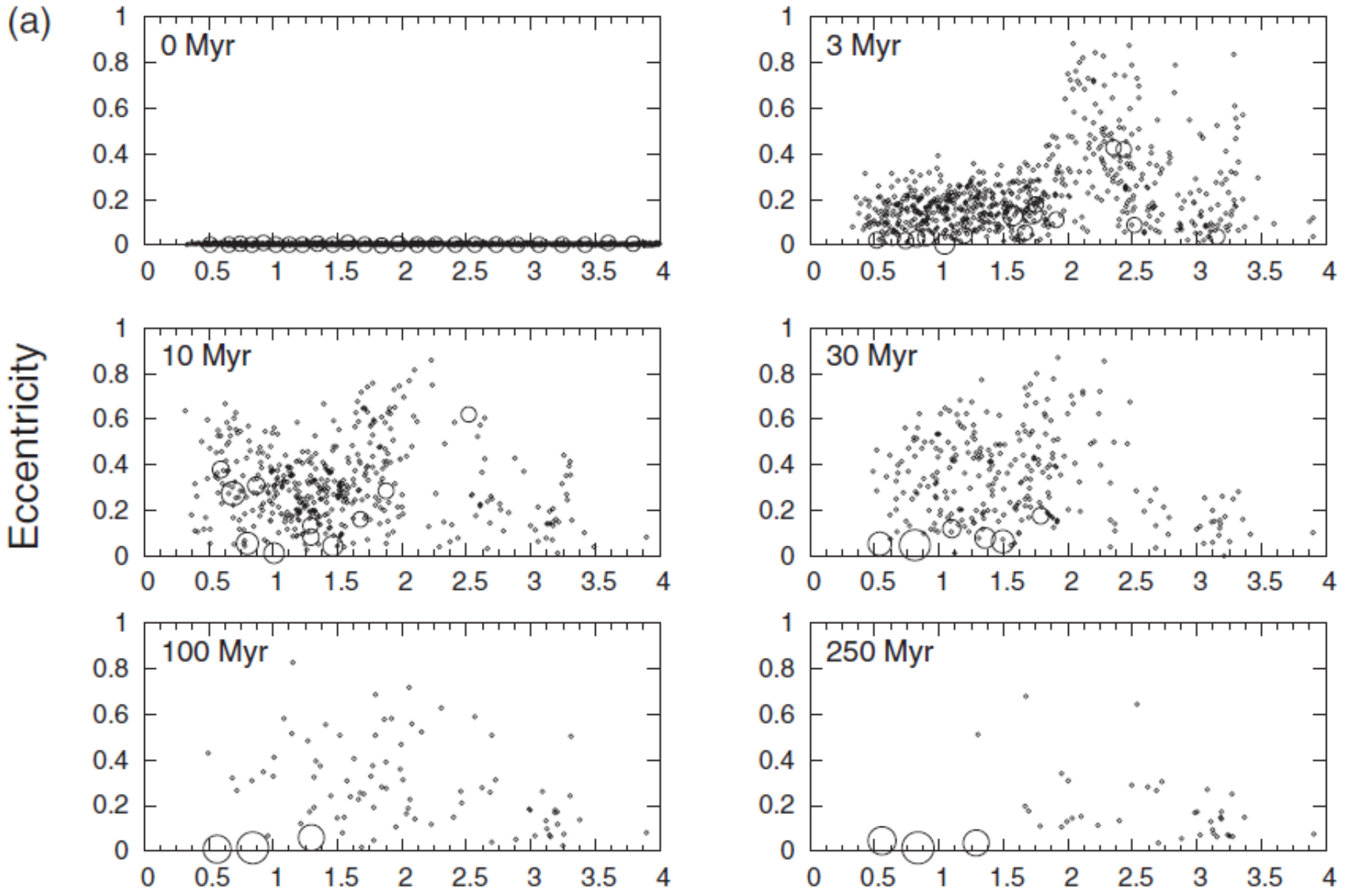
(a)
0 Myr
3 Myr
10 Myr
30 Myr
100 Myr
250 Myr
Eccentricity
Semimajor Axis (AU)
0
0.2
0.4
0.6
0.8
1
0
0.5
1
1.5
2
2.5
3
3.5
4

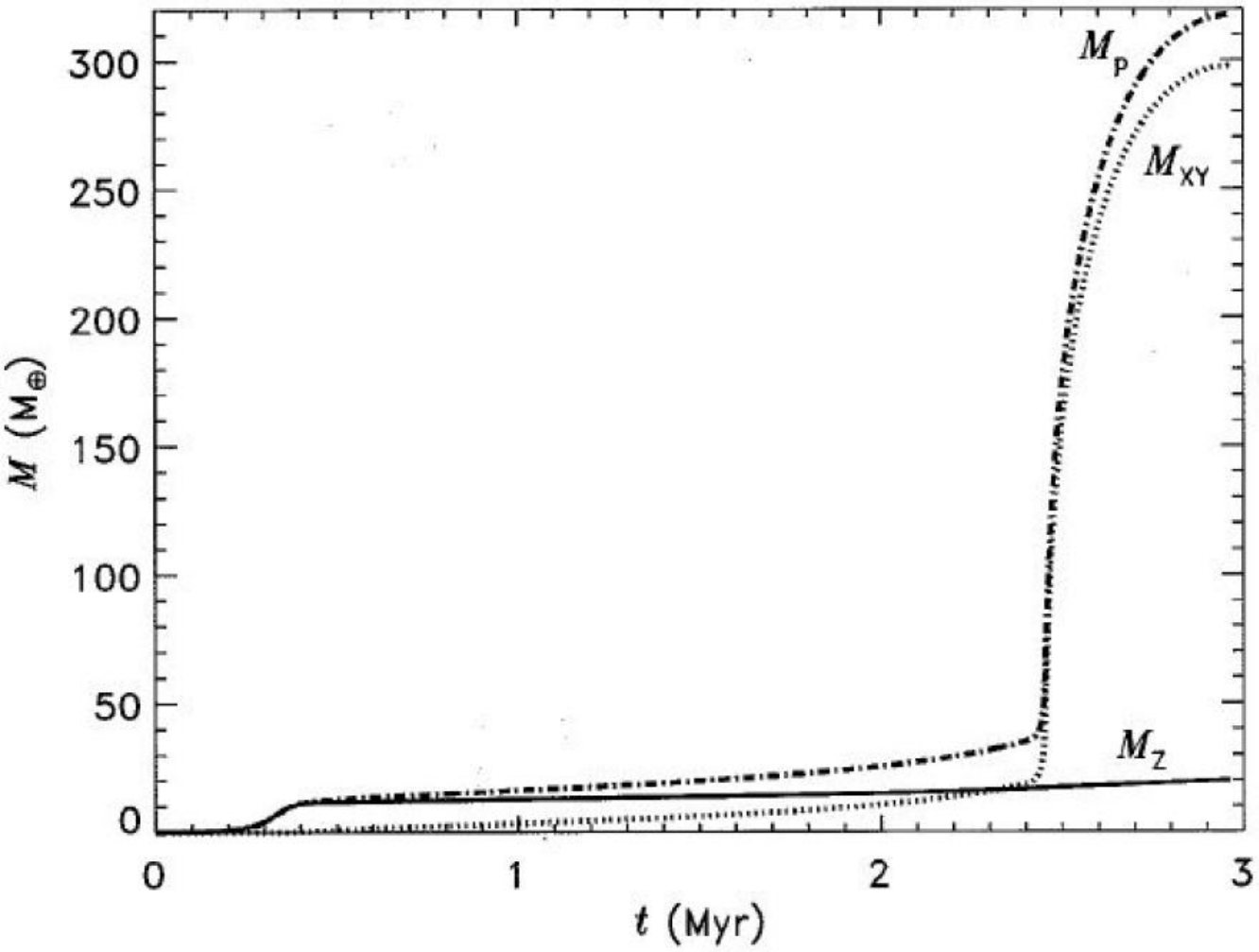

Figure 13.22 The mass of a giant planet that grows to 1 M_J is shown as a function of time according to one particular simulation based upon the core nucleated accretion model. The planet's total mass is represented by the dot-dashed curve, the mass of the solid component is given by the solid curve, and the dotted curve represents the gas mass. The solid core grows rapidly by runaway accretion in the first 4×10^5 years. The rate of solid body accumulation decreases once the planet has accreted nearly all of the condensed material within its gravitational reach. The envelope accumulates gradually, with its settling rate determined by its ability to radiate away the energy of accretion. Eventually, the planet becomes sufficiently cool and massive that gas can be accreted rapidly. This simulation is for growth at 5.2 AU from a 1 $M_\odot$ star, with a local surface mass density of solids equal to 10 g/cm^2. (Lissauer *et al.* 2009)

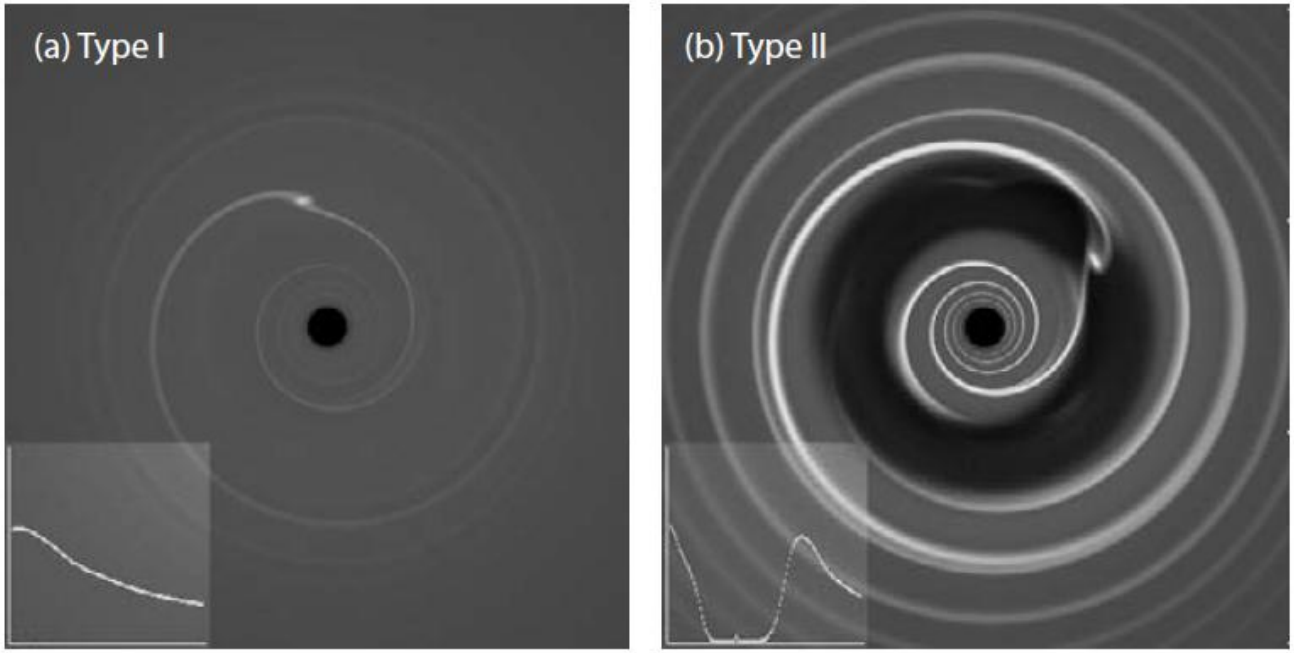

Figure 10.14: Type I and type II migration. Simulations of the interaction between a planet on a circular orbit with a laminar (non-turbulent) protoplanetary disk, computed from a two-dimensional isothermal hydrodynamic code with a constant kinematic viscosity: (a) in type I migration, a relatively low-mass planet excites a wave in the gas disk, but does not significantly perturb the azimuthally-averaged surface density profile (inset); (b) in type II migration, a more massive planet (here of $10 M_{\rm J}$) clears an annular gap, within which the surface density is a small fraction of its unperturbed value. As the disk evolves, the planet follows the motion of the gas (either inward or outward) while remaining within the gap. From Armitage & Rice (2005, Figure 1).

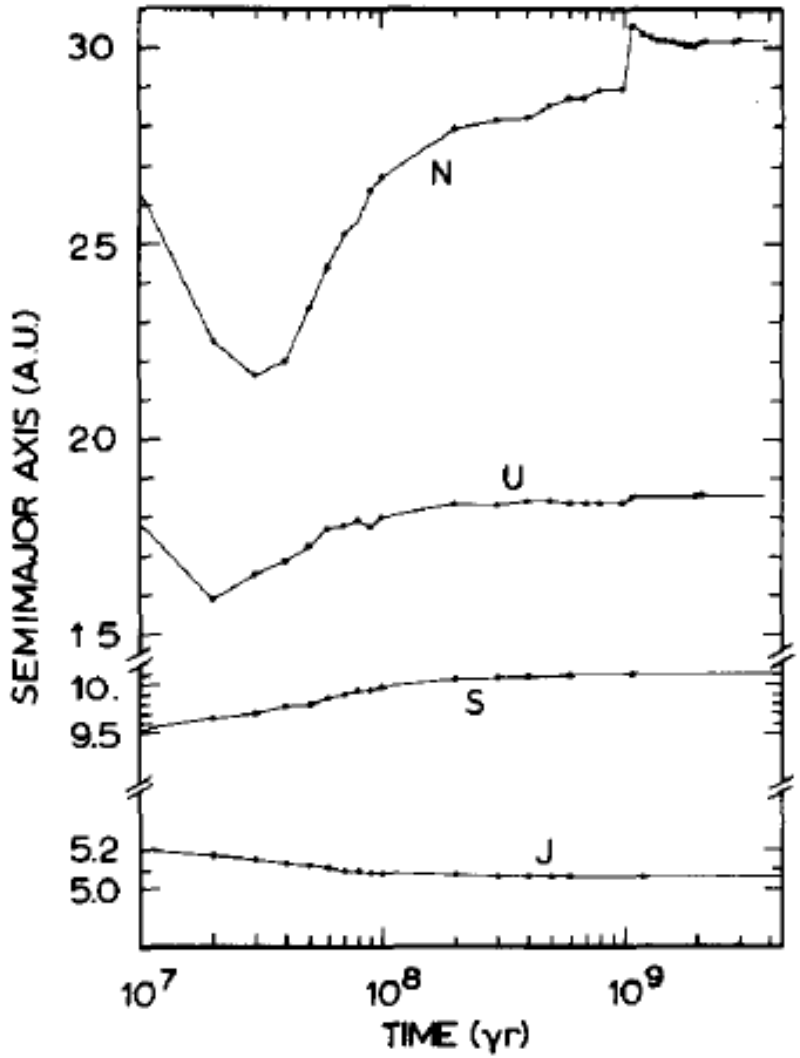

FIG. 3. Time variation of the semimajor axes of the four Jovian planets as a result of exchange of angular momentum with planetesimals. These results are taken from case 7. The initial semimajor axes are a_J = 5.203 AU, a_S = 9.54 AU, a_U = 20 AU and a_N = 30 AU.

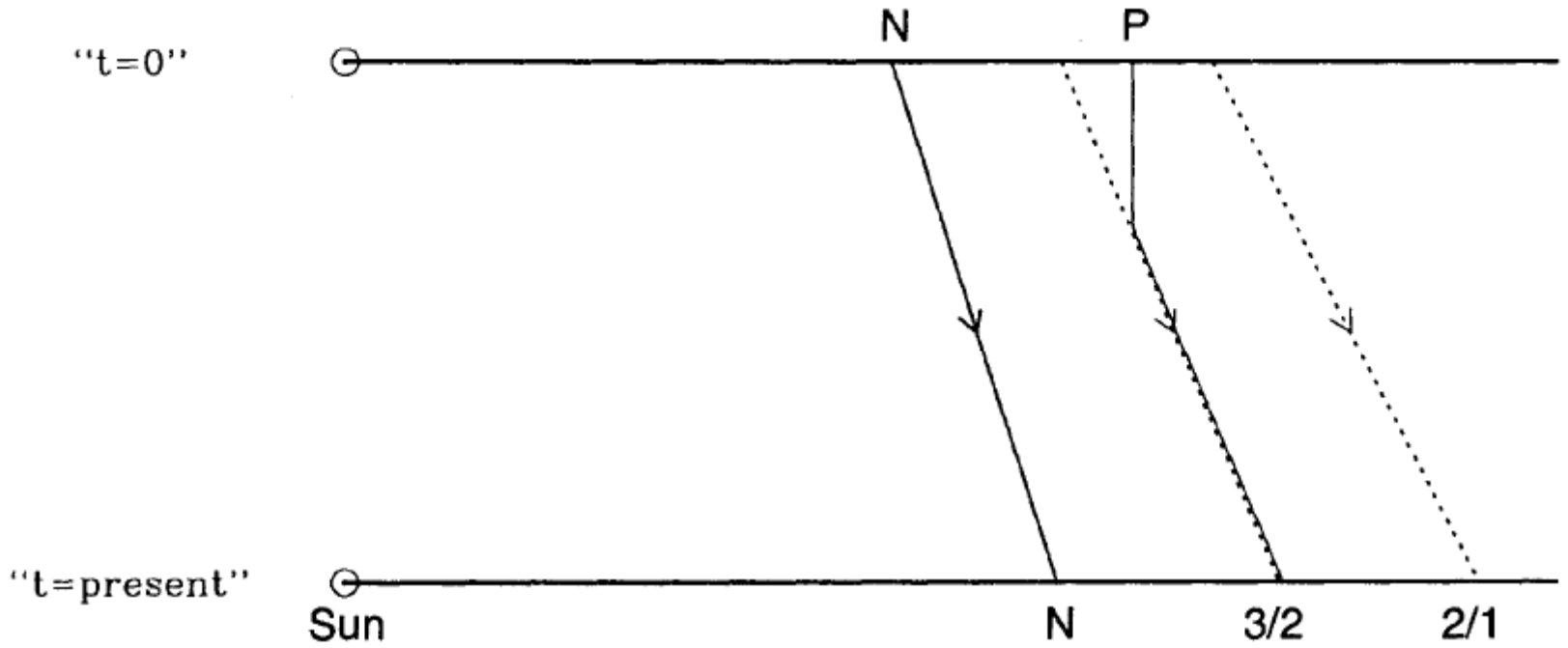

FIG. 1. A schematic diagram to illustrate the outward radial migration of Neptune and its exterior orbital resonances during the late stages of planet formation. The distance from the Sun is along the horizontal direction. Neptune's outward orbital migration is shown along the path marked N–N. For clarity, only two first-order resonances (3:2 and 2:1) are shown (dotted lines). A "Pluto" in an initially circular, nonresonant orbit beyond Neptune could have been captured into the 3:2 resonance and would evolve along the solid line path indicated by P—3/2.

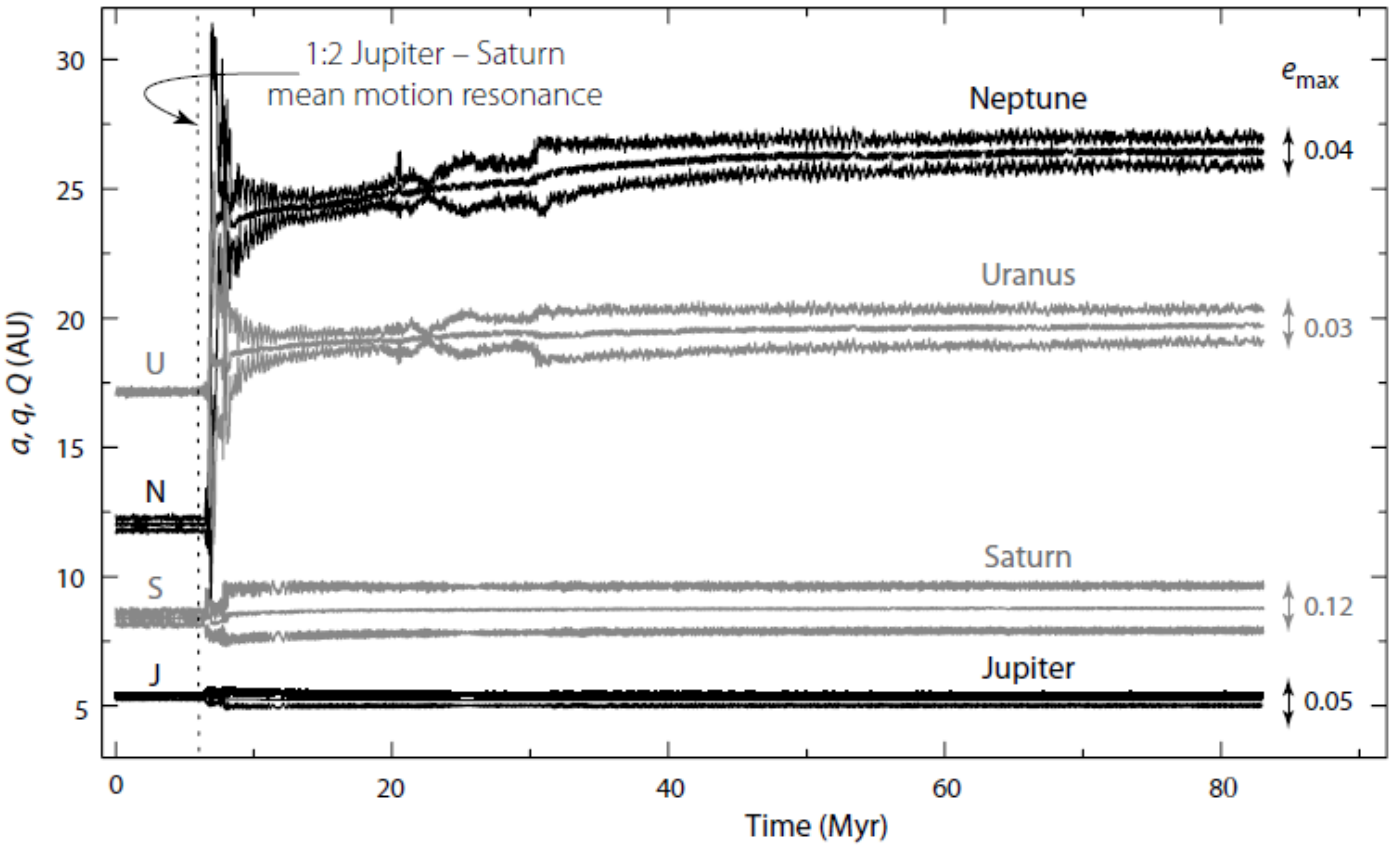

Figure 12.4: The starting configuration of the outer solar system planets given by the Nice model, with their subsequent orbital evolution from an N-body simulation with $35 M_{\oplus}$ of disk planetesimals in 3500 particles out to 30 AU. The three curves for each planet indicate the semi-major axis a, and their minimum (q) and maximum (Q) heliocentric distances. The vertical dashed line marks the epoch of the 1:2 Jupiter–Saturn mean motion resonance capture. During subsequent dynamical interactions, the eccentricities of Uranus and Neptune can exceed 0.5, and in 50% of simulation runs (including this), they exchange orbits. The maximum eccentricity over the last 2 Myr of evolution is indicated. From Tsiganis et al. (2005, Figure 1), by permission from Macmillan Publishers Ltd, Nature, ©2005.

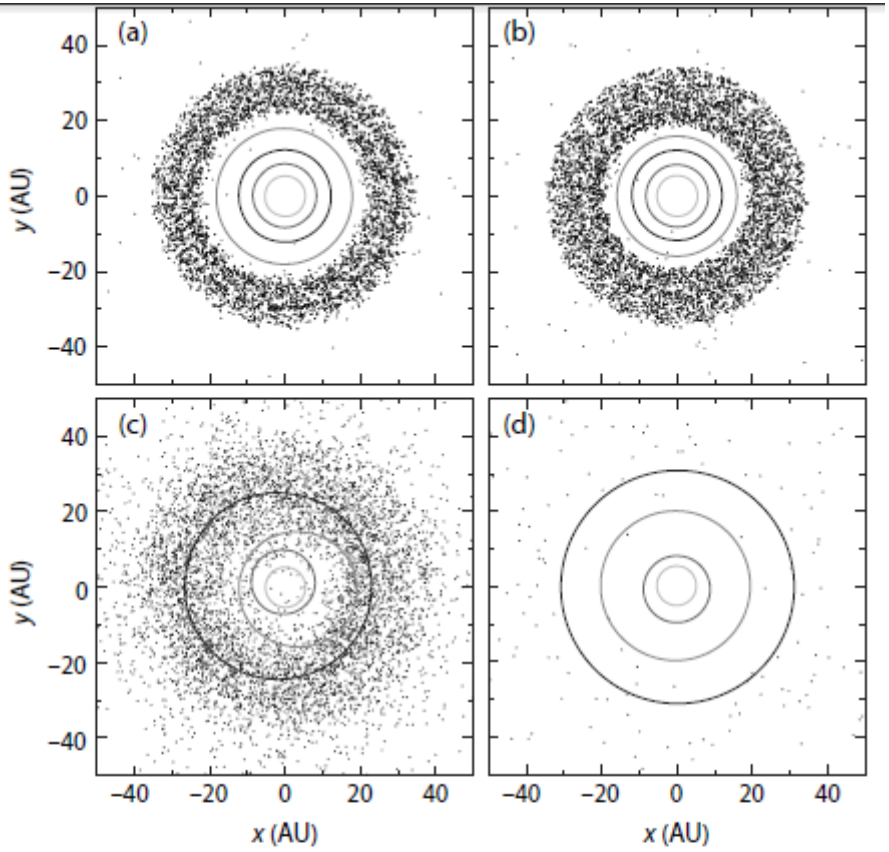

Figure 12.5: Numerical simulations of the lunar heavy bombardment. Planetary orbits and disk planetesimals are projected on the initial mean orbital plane. The four giant planets were initially on nearly circular coplanar orbits, with a = 5.45, 8.18, 11.5 and 14.2 AU, and the planetesimal disk, of total mass $35 M_{\oplus}$, extended from 15.5–34 AU. Panels represent the system at (a) the start of planetary migration (100 Myr); (b) just before the start of the lunar heavy bombardment (879 Myr); (c) just after its start (882 Myr); and (d) 200 Myr later when only 3% of the initial disk mass remains, and the planets have achieved their final orbits. From Gomes et al. (2005, Figure 2), by permission from Macmillan Publishers Ltd, Nature, ©2005.

SISTEMA SOLAR

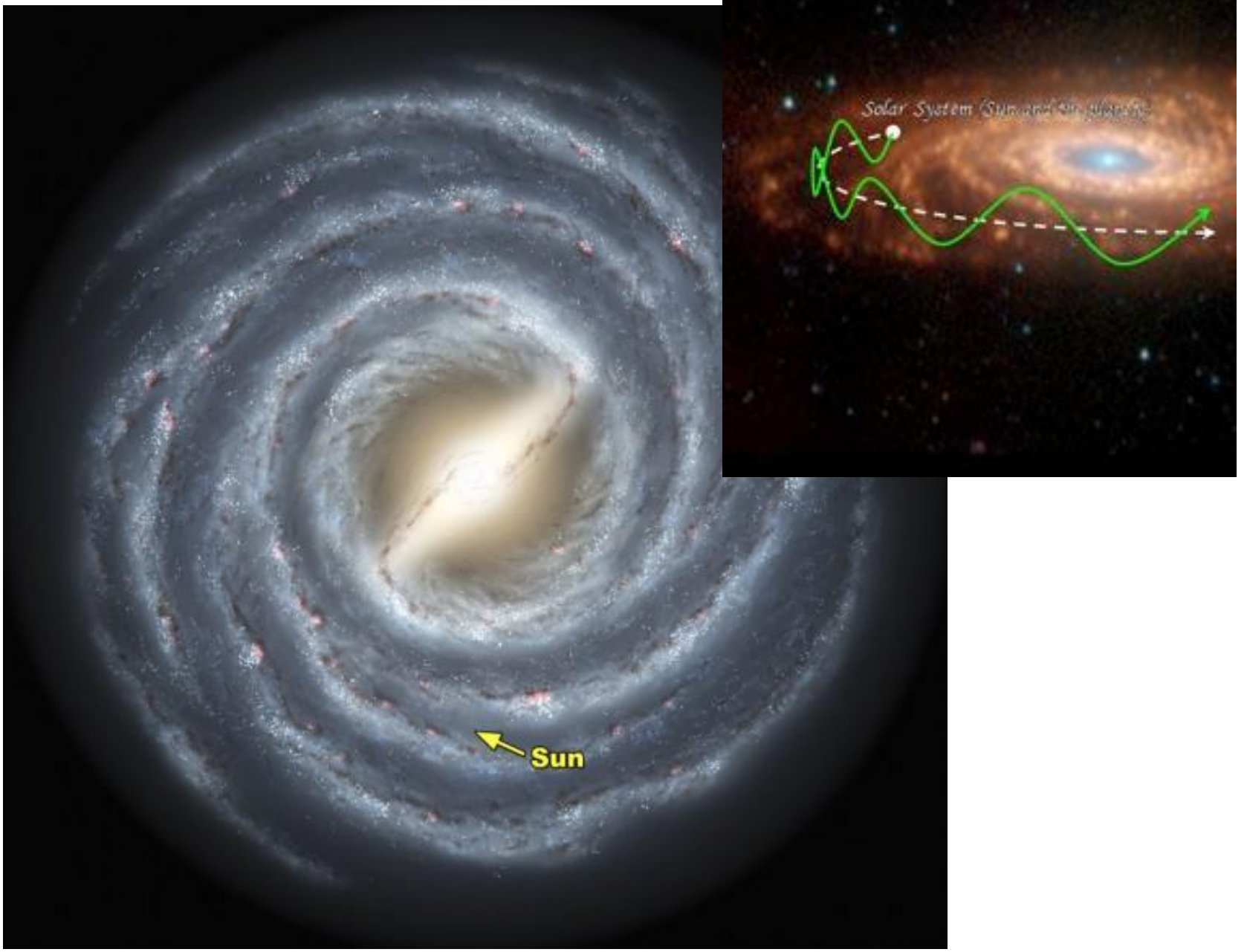
Solar System (Sun and its planets)
Sun

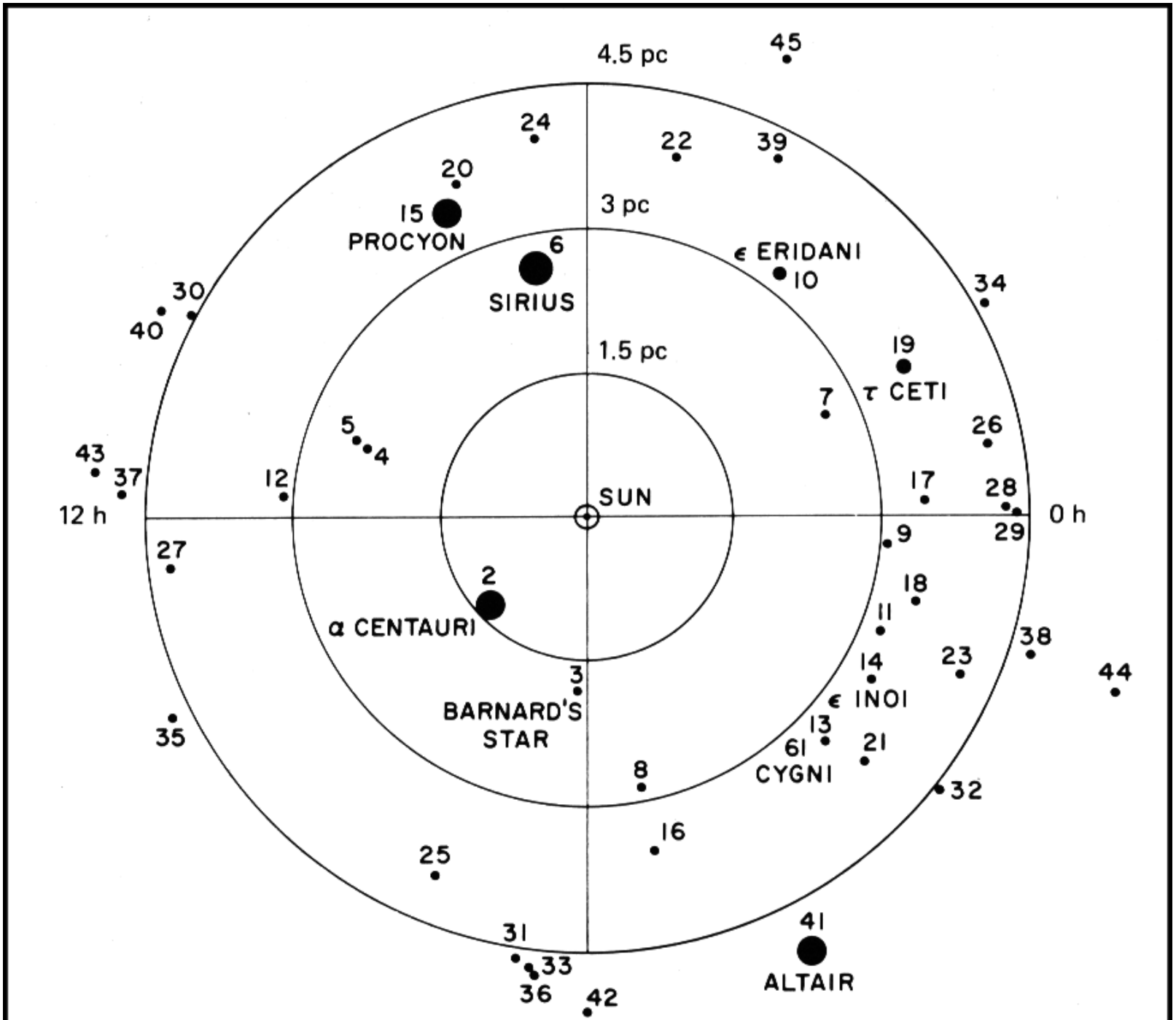
4.5 pc
3 pc
1.5 pc
0 h
12 h
SUN
PROCYON
SIRIUS
ϵ ERIDANI
τ CETI
α CENTAURI
BARNARD'S STAR
ϵ INOI
61 CYGNI
ALTAIR
45
24
22
39
20
15
6
10
34
30
40
19
7
5
4
26
43
37
12
17
28
29
27
9
2
18
11
38
14
23
44
3
35
13
21
8
32
16
25
41
31
33
36
42

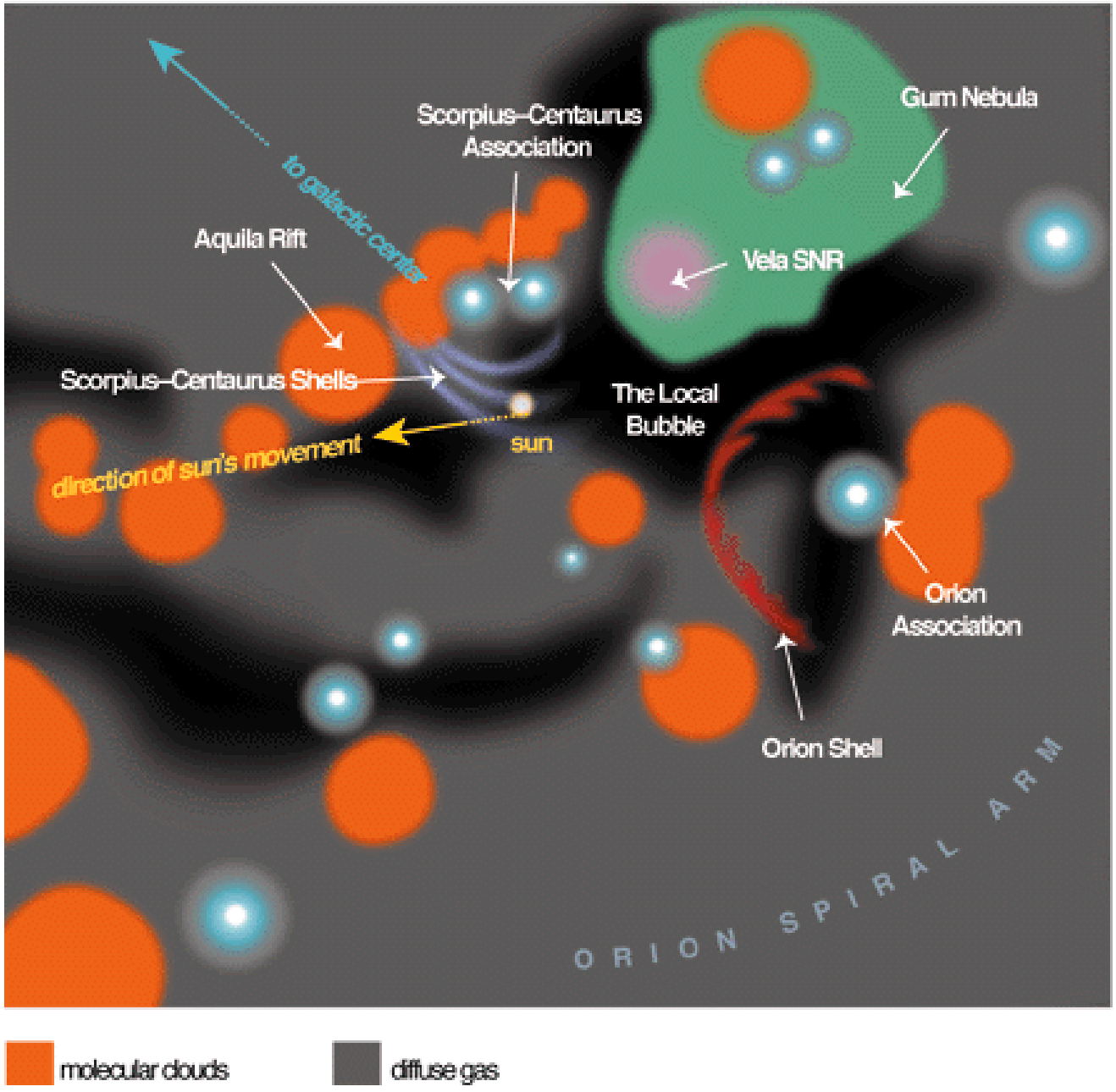
to galactic center
Scorpius–Centaurus Association
Gum Nebula
Aquila Rift
Vela SNR
Scorpius–Centaurus Shells
The Local Bubble
sun
direction of sun's movement
Orion Association
Orion Shell
ORION SPIRAL ARM
molecular clouds
diffuse gas

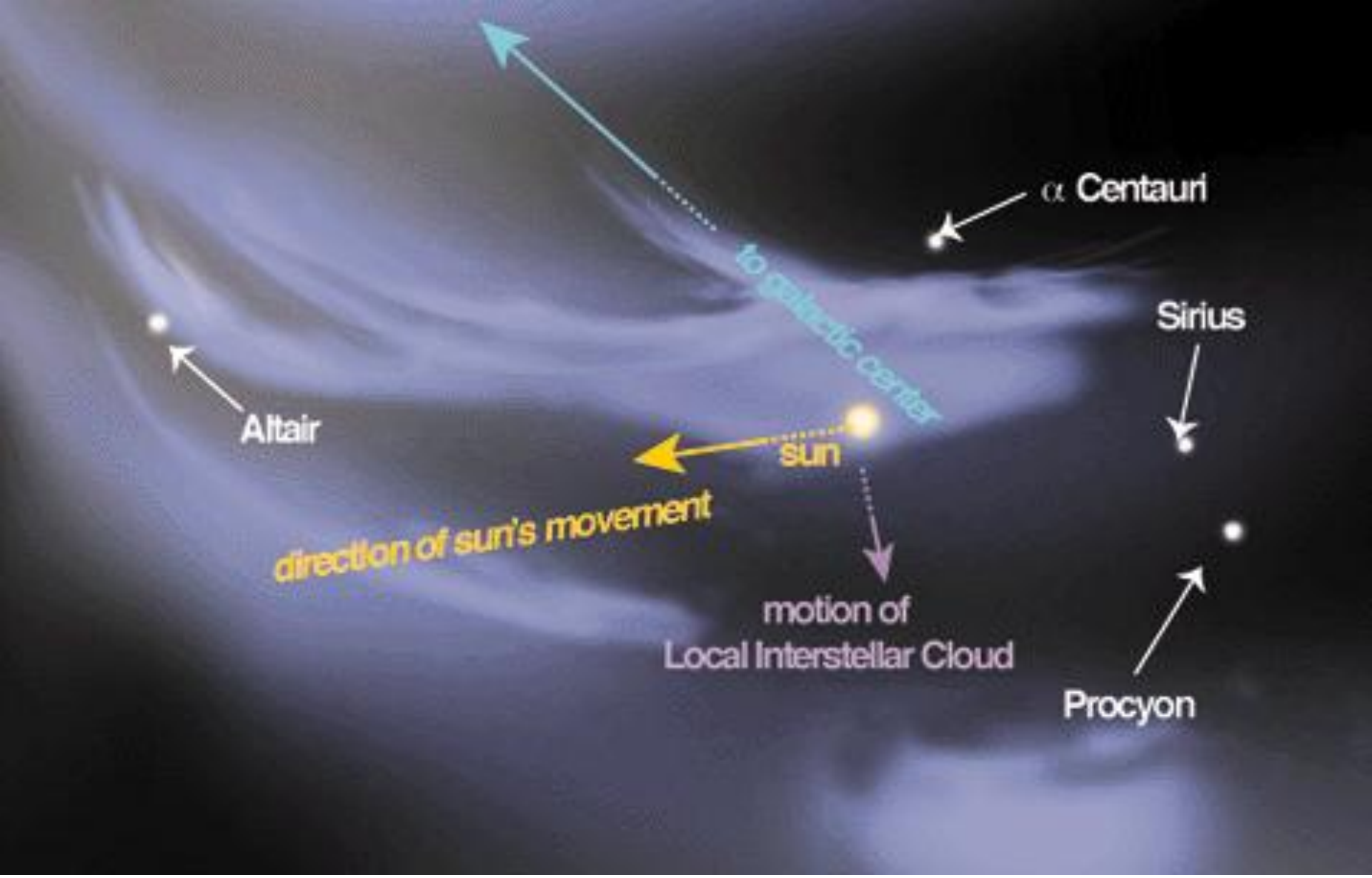
α Centauri
to galactic center
Sirius
Altair
sun
direction of sun's movement
motion of
Local Interstellar Cloud
Procyon

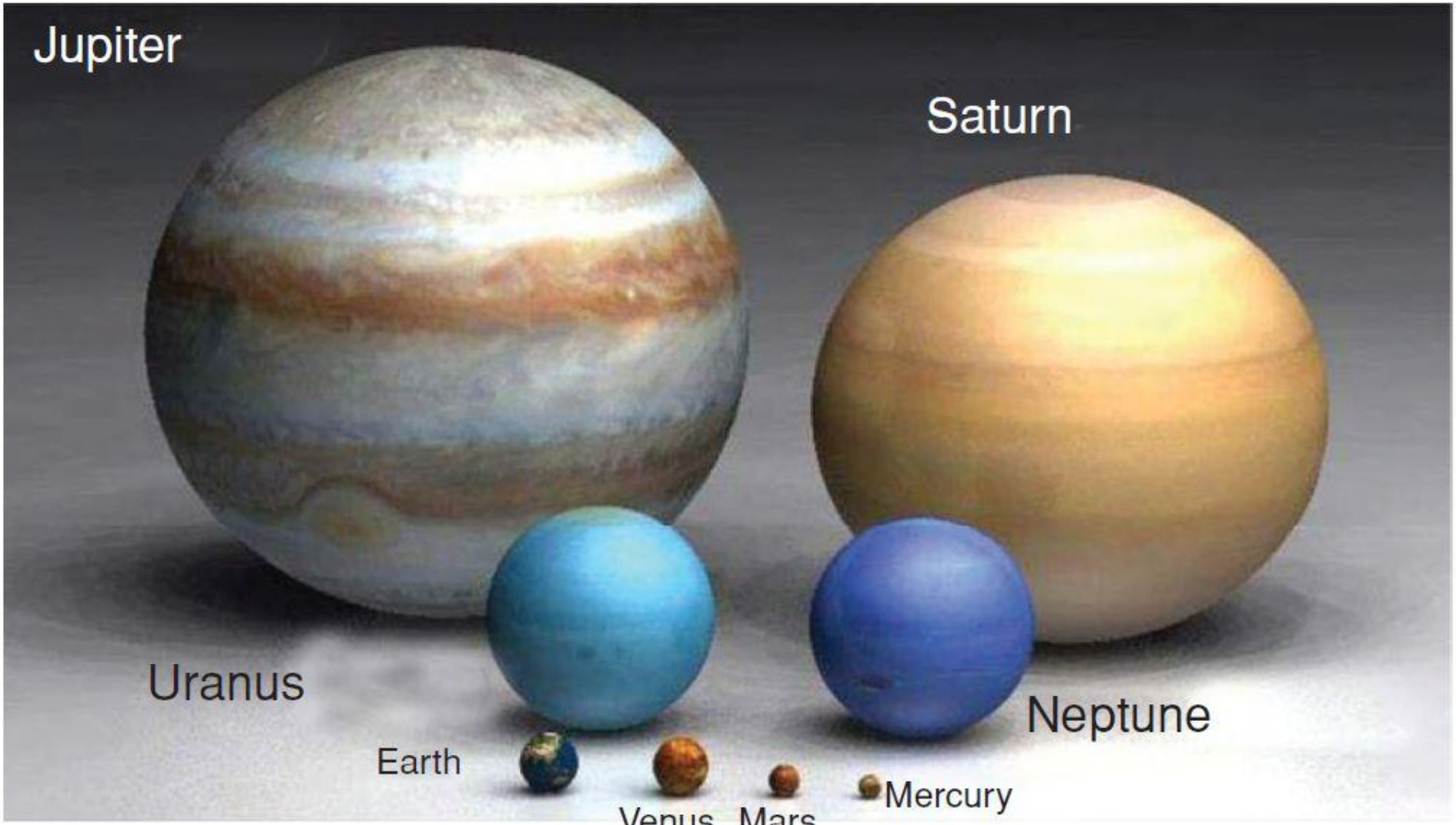
Jupiter
Saturn
Uranus
Neptune
Earth
Venus
Mars
Mercury

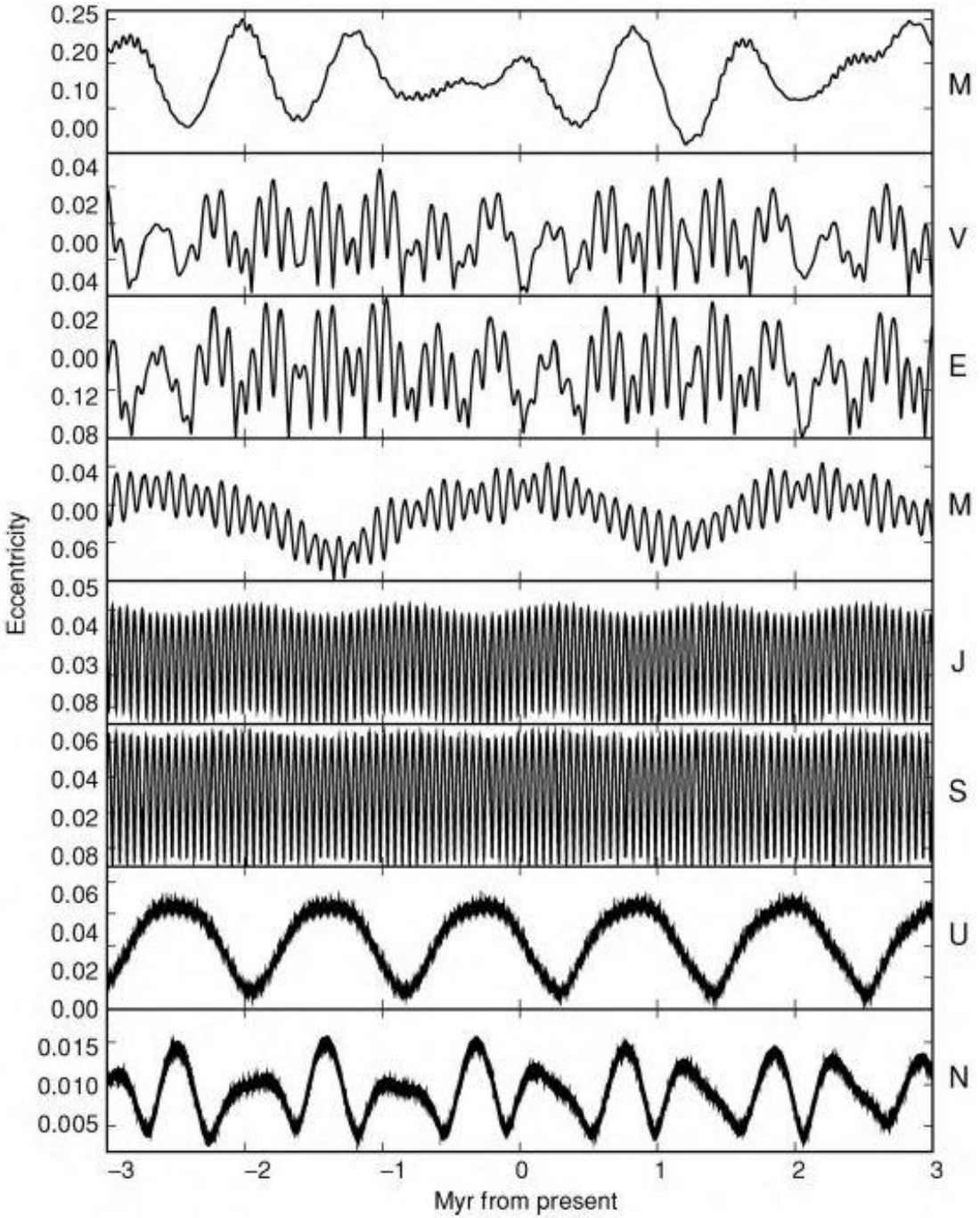
Eccentricity
0.25
0.20
0.10
0.00
M
0.04
0.02
0.00
0.04
V
0.02
0.00
0.12
0.08
E
0.04
0.00
0.06
M
0.05
0.04
0.03
0.08
J
0.06
0.04
0.02
0.08
S
0.06
0.04
0.02
0.00
U
0.015
0.010
0.005
N
−3
−2
−1
0
1
2
3
Myr from present

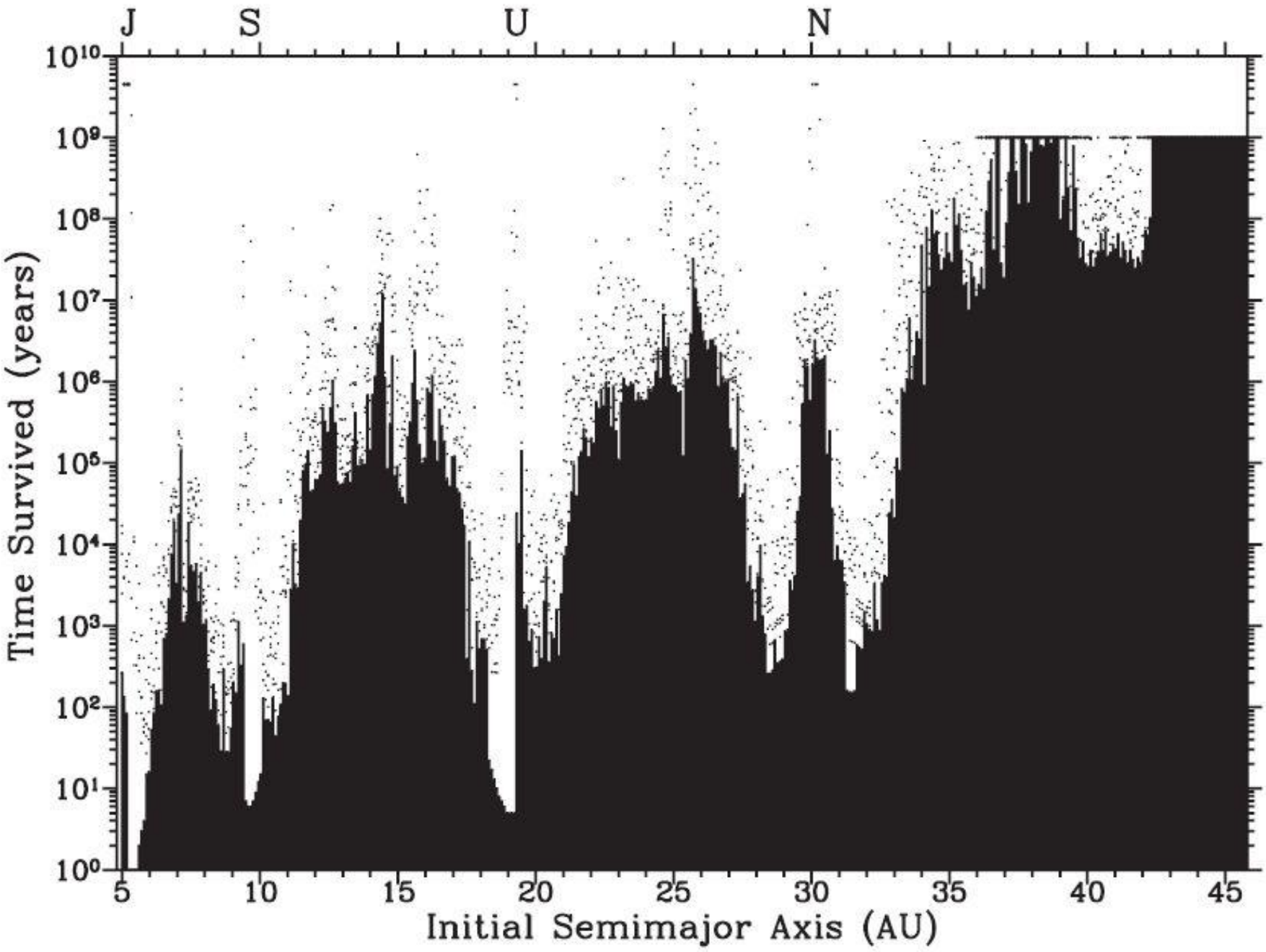
J
S
U
N
Time Survived (years)
Initial Semimajor Axis (AU)

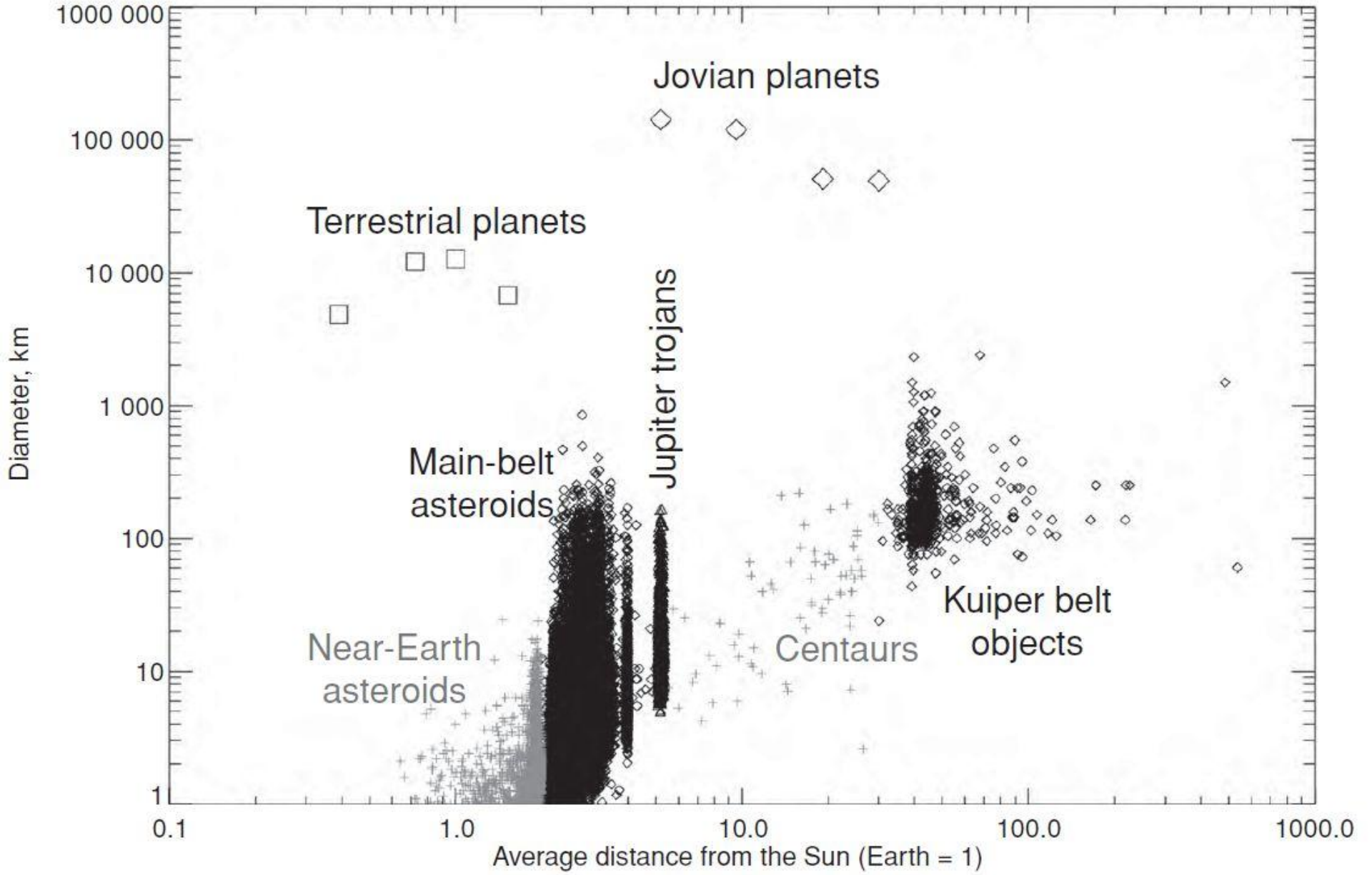
1000 000
100 000
10 000
1 000
100
10
1
Diameter, km
0.1
1.0
10.0
100.0
1000.0
Average distance from the Sun (Earth = 1)
Jovian planets
Terrestrial planets
Jupiter trojans
Main-belt asteroids
Near-Earth asteroids
Centaurs
Kuiper belt objects

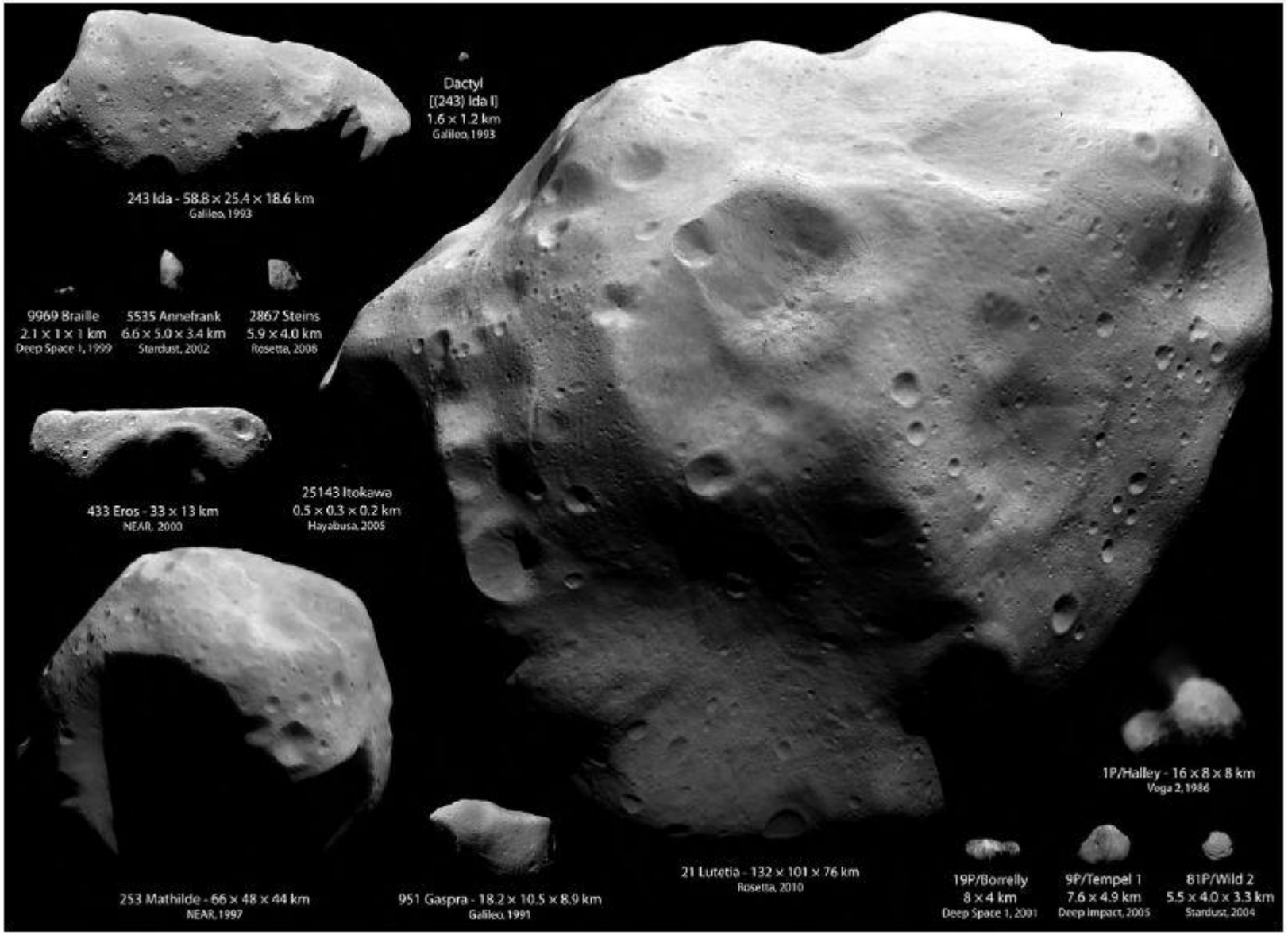
Dactyl
[(243) Ida I]
1.6 × 1.2 km
Galileo, 1993
243 Ida - 58.8 × 25.4 × 18.6 km
Galileo, 1993
9969 Braille
2.1 × 1 × 1 km
Deep Space 1, 1999
5535 Annefrank
6.6 × 5.0 × 3.4 km
Stardust, 2002
2867 Steins
5.9 × 4.0 km
Rosetta, 2008
433 Eros - 33 × 13 km
NEAR, 2000
25143 Itokawa
0.5 × 0.3 × 0.2 km
Hayabusa, 2005
1P/Halley - 16 × 8 × 8 km
Vega 2, 1986
253 Mathilde - 66 × 48 × 44 km
NEAR, 1997
951 Gaspra - 18.2 × 10.5 × 8.9 km
Galileo, 1991
21 Lutetia - 132 × 101 × 76 km
Rosetta, 2010
19P/Borrelly
8 × 4 km
Deep Space 1, 2001
9P/Tempel 1
7.6 × 4.9 km
Deep Impact, 2005
81P/Wild 2
5.5 × 4.0 × 3.3 km
Stardust, 2004

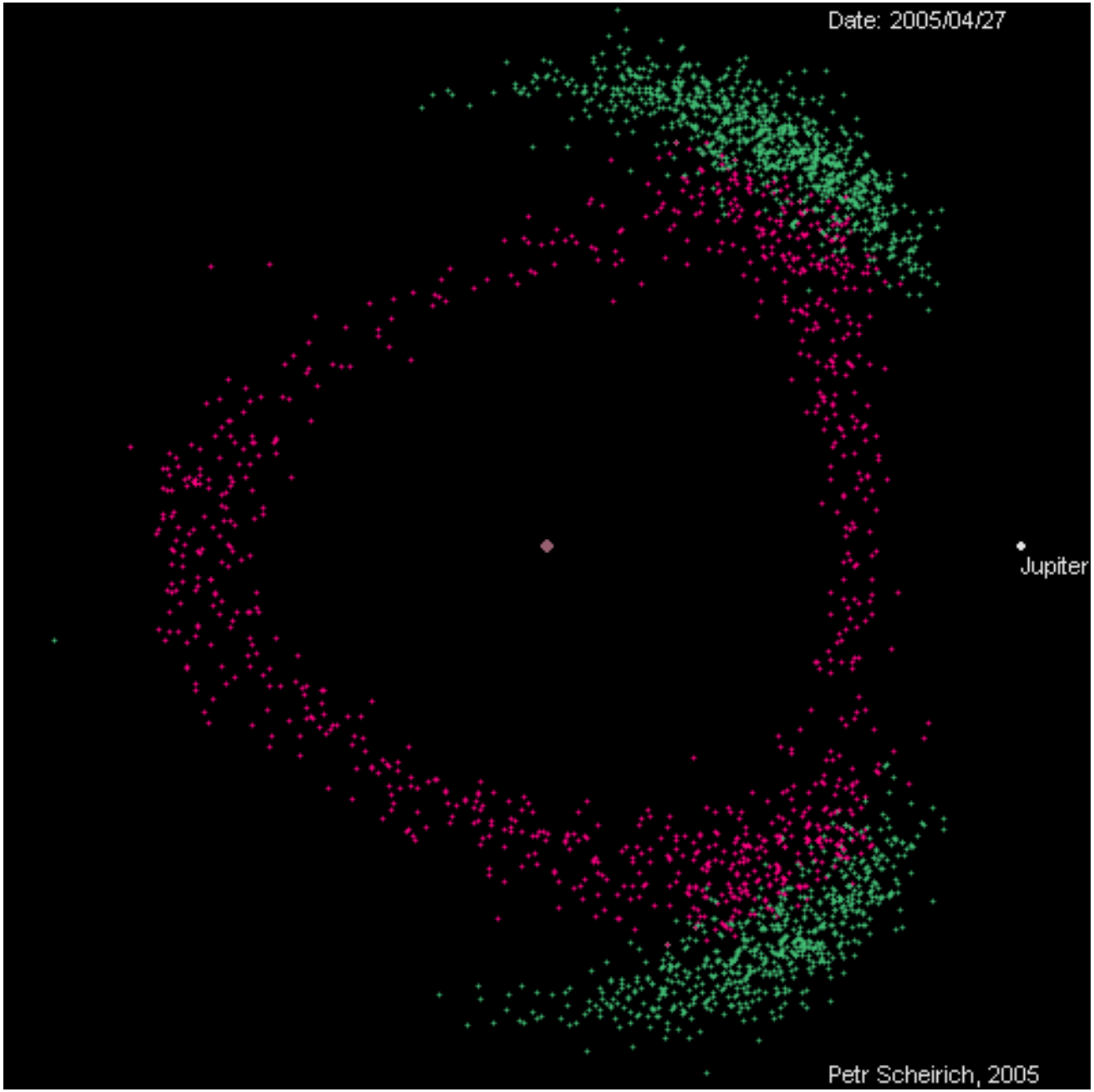
Date: 2005/04/27
Jupiter
Petr Scheirich, 2005

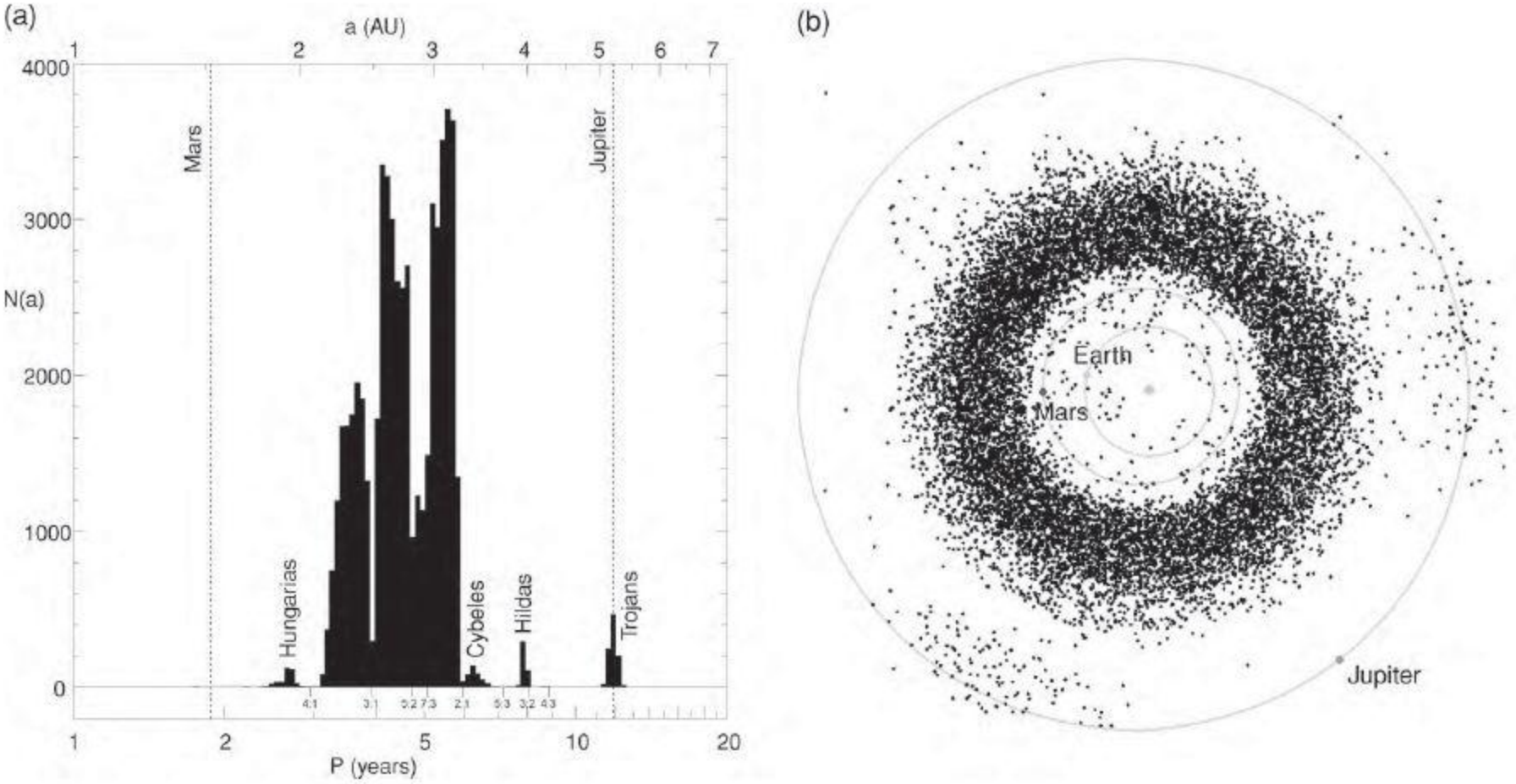

Figure 12.2 (a) Histogram of asteroids versus orbital period (with corresponding semimajor axes shown on the upper scale); the scale of the abscissa is logarithmic. All of the asteroids represented have $M_v < 15$; the 100 000 such asteroids with the smallest numbers are included. The planets Mars and Jupiter are shown by *dashed vertical lines*. Note the prominent gaps in the distribution for orbital periods 1/4, 1/2, 2/5, 3/7 and 1/3 that of Jupiter. One asteroid, Thule, is located at the 4:3 resonance. (Courtesy A. Dobrovolskis) (b) Locations projected onto the ecliptic plane of approximately 7000 asteroids on 7 March 1997. The orbits and locations of the Earth, Mars and Jupiter are indicated, and the Sun is represented by the dot in the center. (Courtesy Minor Planet Center)

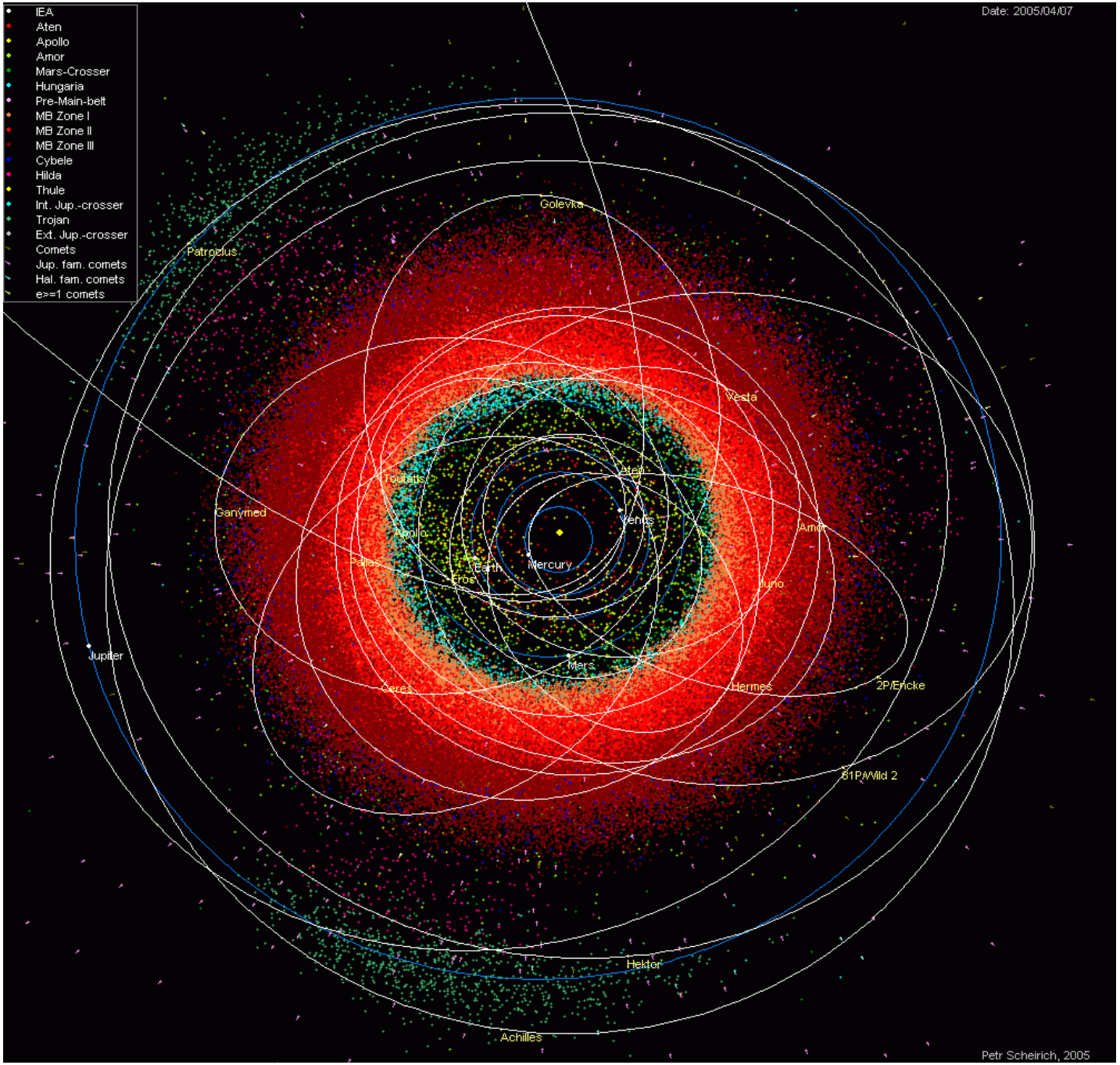
IEA
Aten
Apollo
Amor
Mars-Crosser
Hungaria
Pre-Main-belt
MB Zone I
MB Zone II
MB Zone III
Cybele
Hilda
Thule
Int. Jup.-crosser
Trojan
Ext. Jup.-crosser
Comets
Jup. fam. comets
Hal. fam. comets
e>=1 comets
Date: 2005/04/07
Golevka
Patroclus
Vesta
Toutatis
Aten
Ganymed
Venus
Apollo
Amor
Sun
Earth
Eros
Mercury
Juno
Jupiter
Mars
Ceres
Hermes
2P/Encke
81P/Wild 2
Hektor
Achilles
Petr Scheirich, 2005

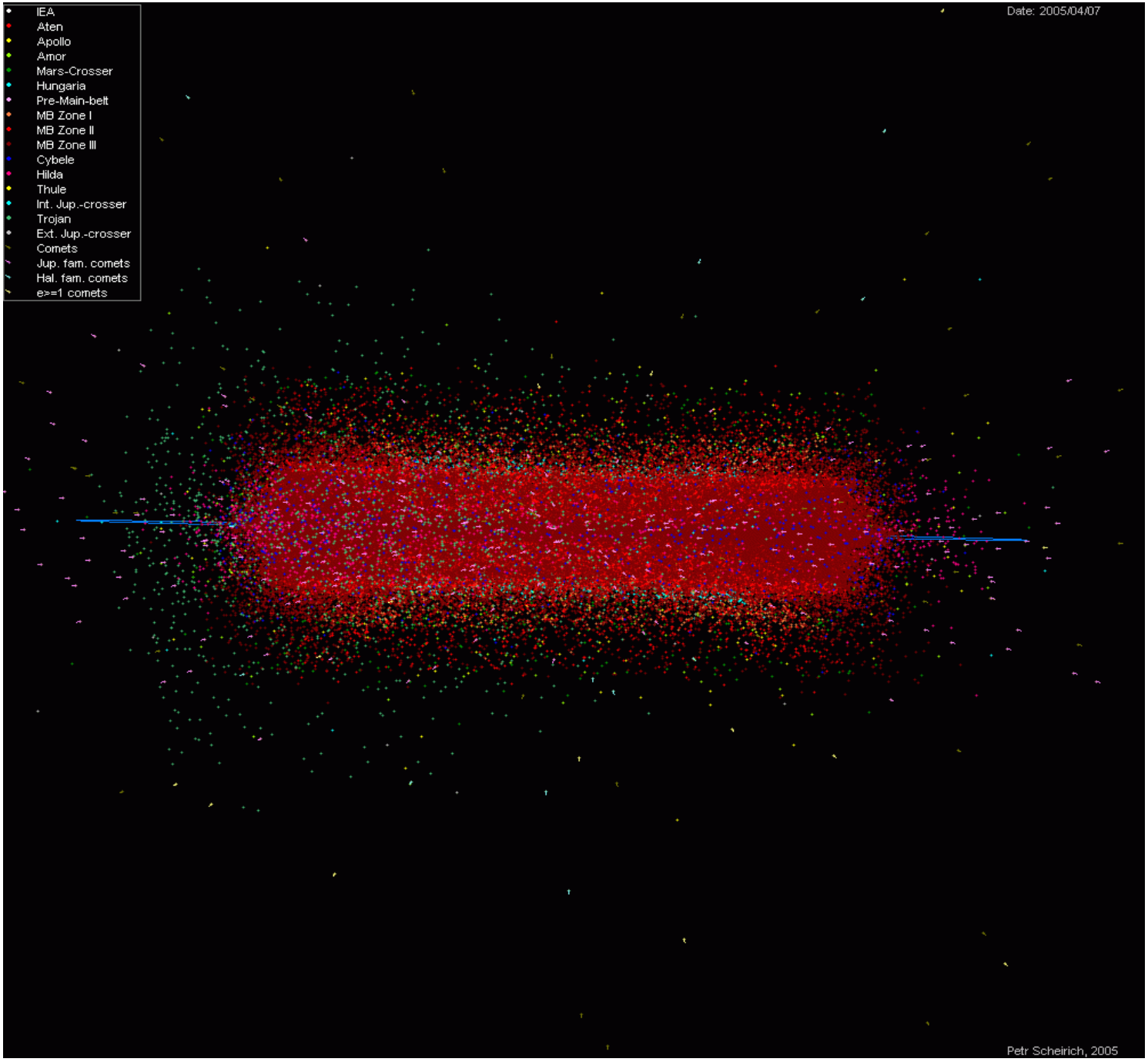
IEA
Aten
Apollo
Amor
Mars-Crosser
Hungaria
Pre-Main-belt
MB Zone I
MB Zone II
MB Zone III
Cybele
Hilda
Thule
Int. Jup.-crosser
Trojan
Ext. Jup.-crosser
Comets
Jup. fam. comets
Hal. fam. comets
e>=1 comets
Date: 2005/04/07
Petr Scheirich, 2005

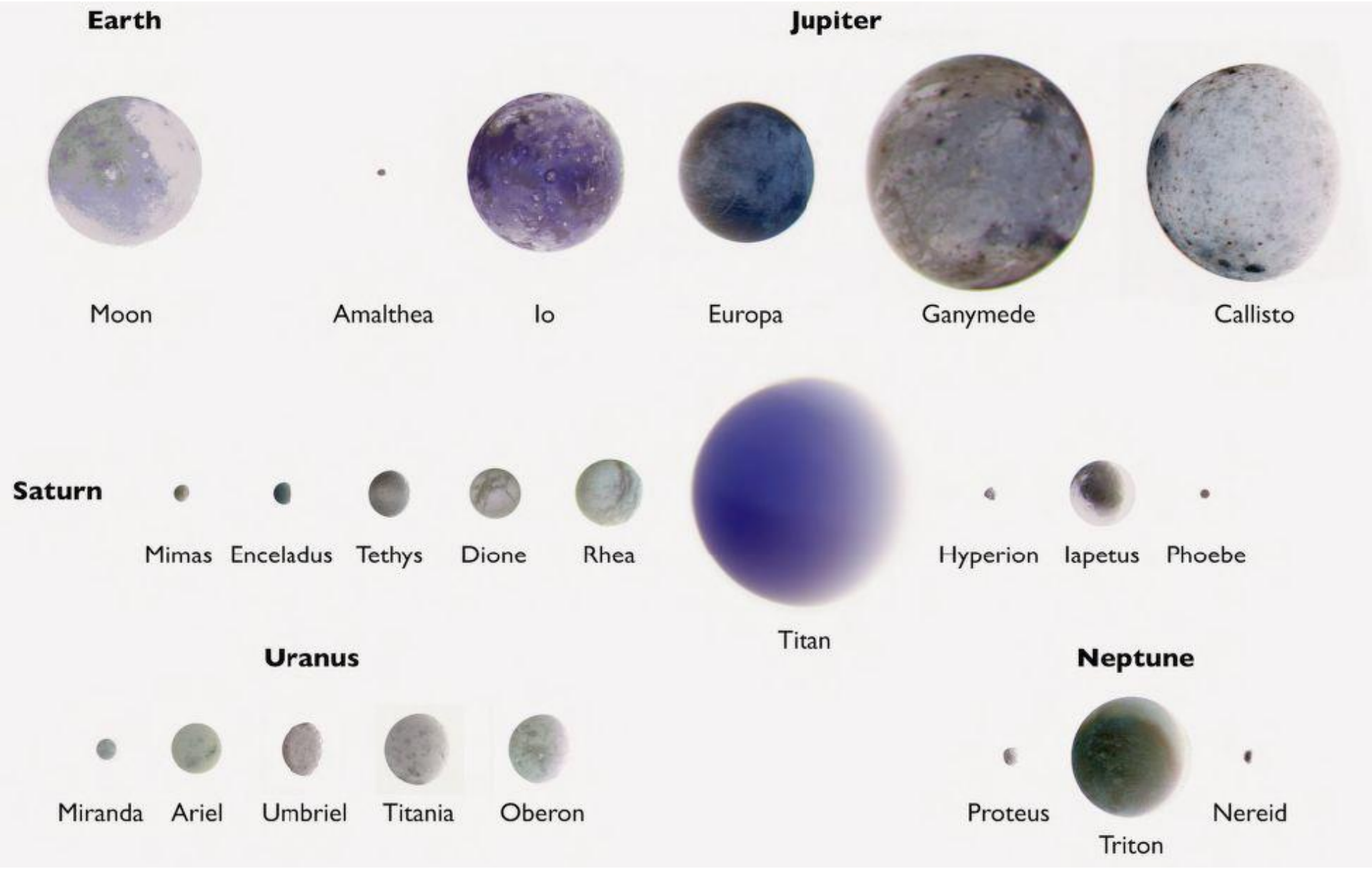
Earth
Jupiter
Moon
Amalthea
Io
Europa
Ganymede
Callisto
Saturn
Mimas
Enceladus
Tethys
Dione
Rhea
Titan
Hyperion
Iapetus
Phoebe
Uranus
Neptune
Miranda
Ariel
Umbriel
Titania
Oberon
Proteus
Triton
Nereid

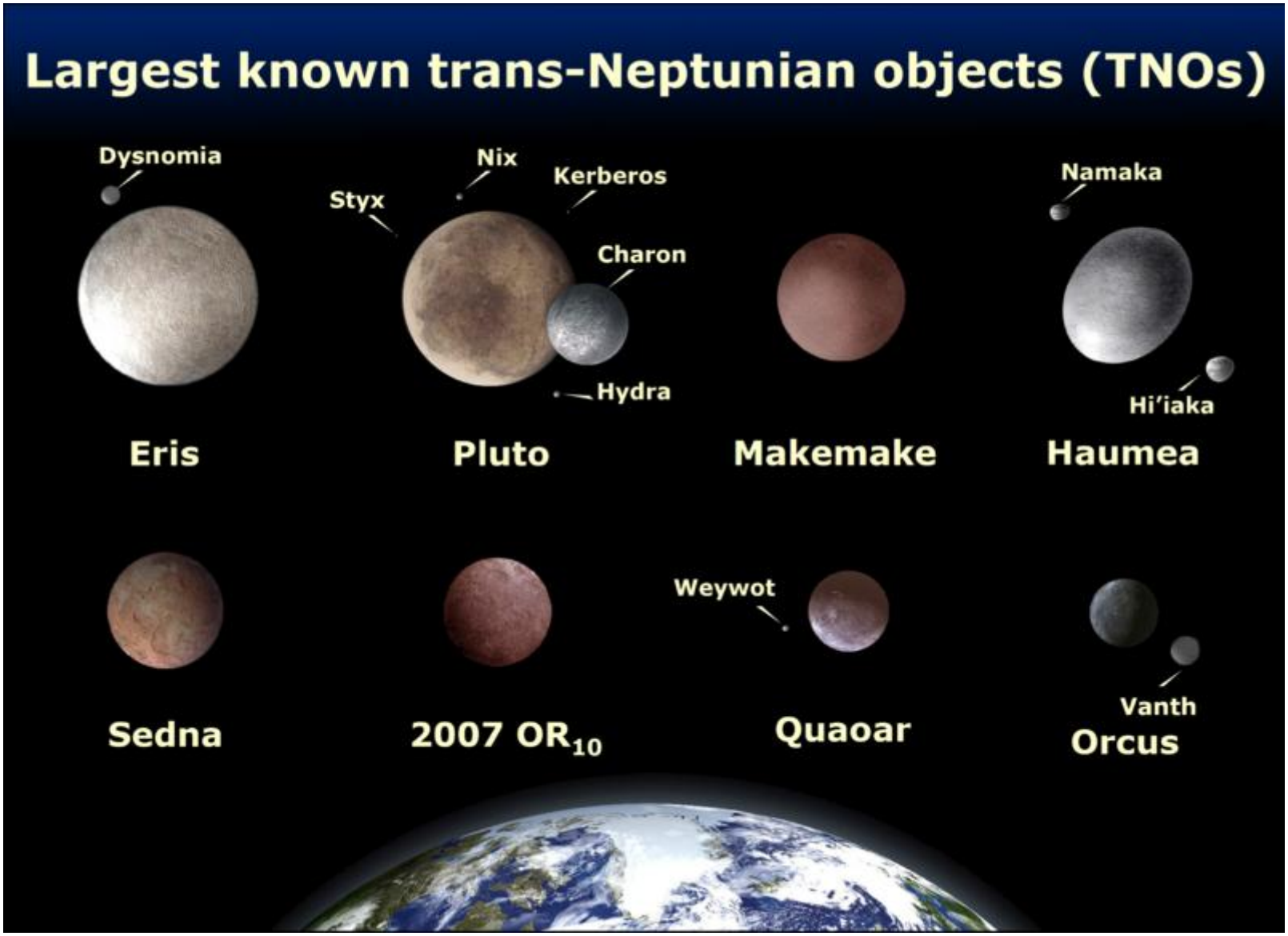
Largest known trans-Neptunian objects (TNOs)
Dysnomia
Eris
Nix
Kerberos
Styx
Charon
Hydra
Pluto
Makemake
Namaka
Hi'iaka
Haumea
Sedna
2007 OR10
Weywot
Quaoar
Vanth
Orcus

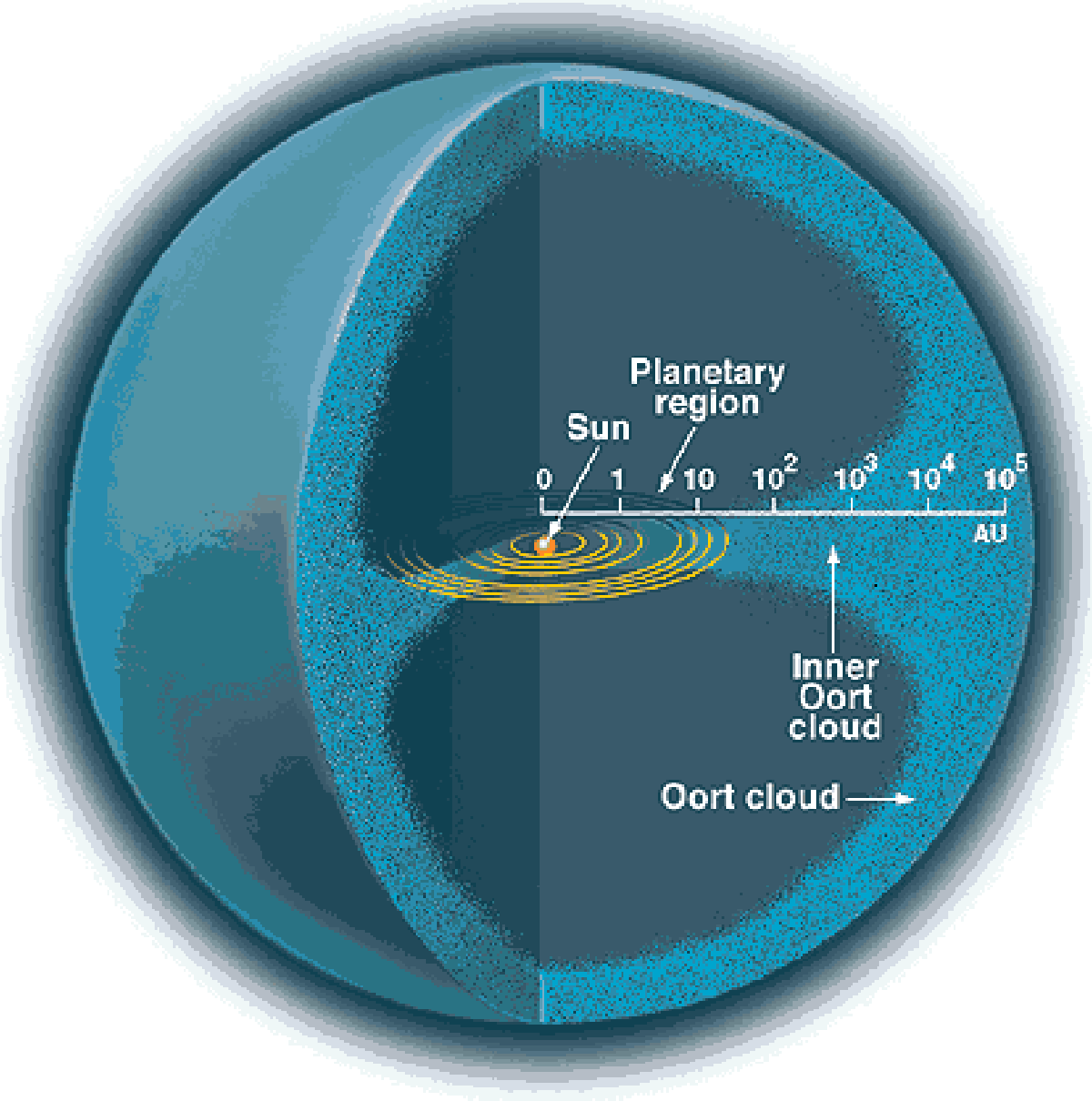
Planetary region
Sun
0
1
10
10^2
10^3
10^4
10^5
AU
Inner Oort cloud
Oort cloud

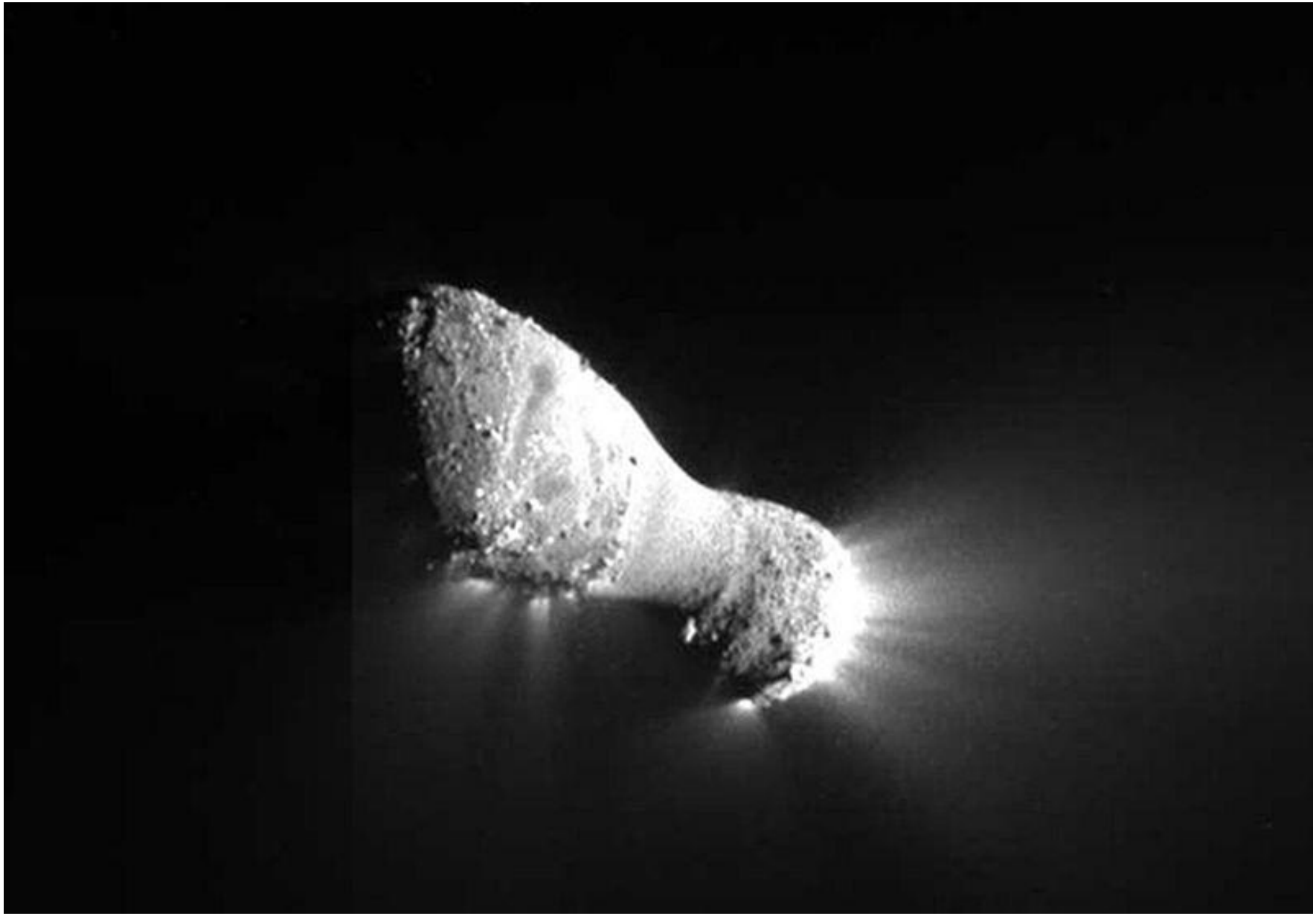

BIBLIOGRAFIA:

- The Exoplanet Handbook, Perryman
- Fundamental Planetary Science, Lissauer y de Pater
- Astrophysics of Planet Formation, Armitage
- exoplanets.org